Numerical analysis of catalysis and ablation effects for carbon-based ablative materials in nitrogen and air plasma environments

D. Bianchi[*†], F. Nasuti[*], M. Onofri[*]
Sapienza University of Rome, Department of Mechanical and Aerospace Engineering
Via Eudossiana 18, 00184, Rome, Italy
D. Le Quang Huy[*] and A. Turchi[*]
von Karman Institute for Fluid Dynamics
Chaussée de Waterloo 72, B-1640, Rhode-St-Genèse, Belgium
[†]Corresponding author: daniele.bianchi@uniroma1.it

Abstract

A numerical strategy based on CFD analysis for the extraction of gas-surface interaction parameters from the results of an experimental campaign performed in the VKI Plasmatron ICP facility has been proposed and assessed. The implemented ablation (i.e. surface oxidation, nitridation and sublimation) and catalysis (i.e. nitrogen recombination and oxygen recombination) models for carbon-based materials are assessed via numerical rebuilding of the experimental tests for different surface conditions in pure nitrogen and air environments and validated against measured data from the experiments. A thorough sensitivity analysis to several parameters that influence the sample ablation/catalysis process has been performed. Finally, a numerical strategy has been defined to derive the effective reaction probabilities for the reactions under scrutiny for both pure nitrogen and air test cases based on the experimentally measured data. Results show that nitridation reaction probability can be derived with very limited scatter, due to its kinetic-limited regime in the test conditions, while oxidation reaction probability is more significantly scattered, being oxidation in a diffusion-limited regime. Recombination probability, finally, appears to be significantly affected by the emissivity measurement errors, especially at high surface temperatures.

1. Introduction

Non-ablating thermal protection systems (TPS) are used on reusable hypersonic vehicles, on the leeward portions of hypersonic vehicles, or for those missions in which the heating rate or the duration of heating are insufficient to cause significant amounts of vaporization or melt flow of the surface material. In this case, surface catalysis is one of the primary mechanisms for transferring energy to the surface of an entry vehicle. Catalytic surface heat transfer occurs when the TPS material at the fluid-surface interface acts as a catalyst to an exothermic reaction involving chemical species impinging the surface from the flow. A fraction of the catalytic energy released at the surface is conducted into the vehicle; the additional heating increases the TPS mass. In Earth atmosphere, atomic oxygen combining to form O_2 or atomic nitrogen combining to form N_2 are important surface catalytic reactions.[9]

Figure 1 shows the radiative equilibrium steady-state temperature as a function of the Mach number for different altitudes. Indeed, metals do not exceed 1500 K and are penalized by a low emissivity. Ceramic composites do not exceed about 2000 K in an oxidizing atmosphere.[8] Therefore, for spacecrafts that have to bear severe entry conditions (e.g., velocity and peak heat flux above 10 km/s and 10 W/cm^2, respectively), engineers cannot prescind, since the early ages of space exploration, from the use of *ablative* materials to build efficient heat shields.[12] Ablative heat shields are able to dissipate the high heat fluxes through chemical and physical decomposition, transforming the thermal energy into mass loss and recession, whilst the remaining solid material insulates the vehicle substructure.[8] The two principal ablative material categories are: 1) non-charring, chemically homogeneous materials which are consumed as a combined result of chemical attack and sublimation at the exposed surface (e.g., graphite, carbon-carbon); 2) composite charring ablative materials which, in addition to surface consumption, decompose in depth to form a high-temperature char layer.[11] To achieve high performance characteristics of ablative materials, mostly composites are used, providing a pyrolyzing, ablating, and insulating material at low weight with reasonable mechanical properties due to a carbon-fiber
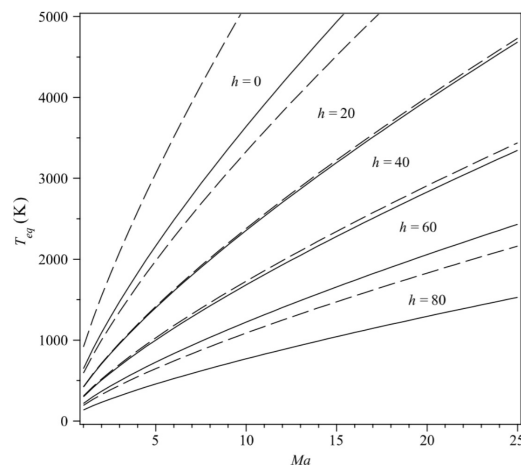
Figure 1: Mach number influence on radiative equilibrium temperature for varying altitudes (in km), from Ref.[8]. Spherical body with 1 m radius. Used emissivities are 0.2 for metals (dashed lines) and 0.8 for ceramic composite (solid lines), respectively.

preform.[15] Examples are phenolic-impregnated carbon ablator (PICA)[17] and ASTERM,[14] developed for high-speed entry missions.

Ground tests of light-weight carbon-based ablative materials in heating conditions relevant to real missions have been performed in the VKI Plasmatron ICP facility in pure nitrogen and air environments. A numerical strategy based on CFD analysis for the extraction of gas-surface interaction parameters from the results of the experimental campaign has been proposed and assessed. In order to perform the numerical simulations, gas-surface-interaction (GSI) models have been implemented into a parallel, multi-block, finite volume three-dimensional code that solves the Navier-Stokes equations for compressible single-phase multicomponent reacting systems, including finite-rate chemistry and variable thermodynamic and transport properties.[6] The implemented ablation (i.e. surface oxidation, nitridation and sublimation) and catalysis (i.e. nitrogen recombination and oxygen recombination) models are assessed via numerical rebuilding of the experimental tests for different surface conditions in pure nitrogen and air environments and validated against measured data from the experiments. A thorough sensitivity analysis to several parameters that influence the sample ablation/catalysis process has been performed, including: Schmidt number, surface emissivity, and surface reaction efficiencies.

Finally, a numerical strategy has been defined to derive, from the CFD solutions, the effective reaction probabilities for the reactions under scrutiny for both pure nitrogen and air test cases based on the experimentally measured data. The results in terms of reconstructed effective reaction probabilities for carbon nitridation, carbon oxidation and nitrogen recombination in different environments are discussed and compared with the available literature data.

2. Theoretical and numerical modeling

This study has been performed with state-of-the-art analysis tools developed by Uniroma with specific application to ablative heat shields for atmospheric reentry vehicles. The ablative boundary conditions have been implemented in a parallel, multi-block, finite volume three-dimensional code that solves the Navier-Stokes equations for compressible single-phase multicomponent reacting systems, including finite-rate chemistry and variable thermodynamic and transport properties. The code, which adopts a standard finite volume Godunov-type formulation, is second order accurate in space uses multi-block structured meshes. The system of equations is approximated by a cell-centered finite volume scheme. The viscous fluxes are approximated by centered differencing, whereas the convective fluxes are computed by means of the solution of a Riemann problem whose left and right states are reconstructed by an interpolation procedure which uses the minmod limiter. The system of ordinary differential equations is advanced in time by means of an explicit Runge-Kutta integration. The flow is assumed to be laminar, in thermal equilibrium, and is modeled with a single-temperature, 6-species and 6-reaction finite-rate chemistry model for nitrogen environments and 11-species and 18-reaction finite-rate chemistry model for air environments. In addition, the code has been parallelized using the OpenMP directives and it can run on SMP computers. The solver has been fully integrated with a customized gas-surface interaction wall boundary condition based on finite-rate heterogeneous surface reactions (including catalytic reactions and surface oxidation, nitridation and sublimation) that allows to calculate ablation mass blowing flux, surface chemical composition and surface temperature as part of the CFD solution. The numerical tool has been validated

and verified for pyrolyzing and non-pyrolyzing ablative materials in published works for both external and internal high-temperature flows.[1–5,7,18]

2.1 Gas-surface interaction wall boundary condition

In the approach proposed in this work, a predicting CFD code is developed where the gas-solid phase coupling is handled through a customized gas-surface interaction wall boundary condition that has been fully integrated within the CFD solver. The ablating material surface represents an interface between the gaseous atmospheric products flowing over the sample and the solid carbon-based material so that the solid and gas-phase boundaries are fully coupled at the interface. The ablating material wall boundary condition is based on mass, species and energy conservation equations as reported in Figs. 2 and 3.
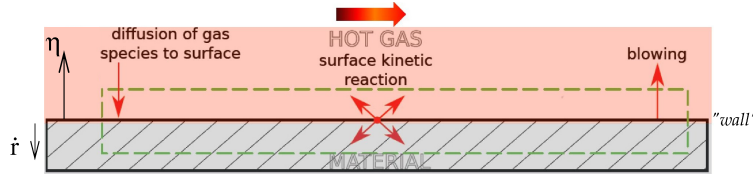
Figure 2: Surface mass balance for an ablating material.
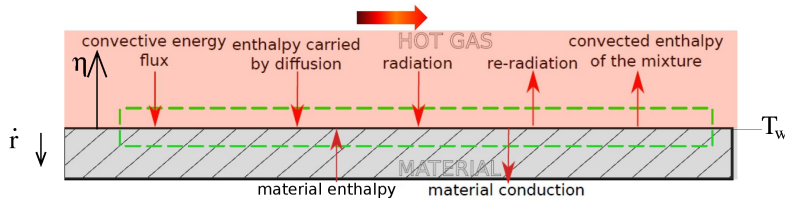
Figure 3: Surface energy balance for an ablating material.

The mass flux of i species (being either atmospheric or ablation/catalysis product) entering the infinitesimal volume by diffusion or production must be balanced by the mass flux leaving the volume by convection (see Fig. 2). A proper surface mass balance is hence fundamental to derive the correct amount of mass entering the flowfield from the ablating surface as well as the thermo-chemical boundary layer characterization which will affect the subsequent evolution of the convective fluxes. Convective and also possibly radiative heat transfer from the boundary layer, in turn, provide the energy for the thermal decomposition of the surface material, through the surface energy balance (see Fig. 3). The energy flux due to i species entering the infinitesimal volume by diffusion, to material enthalpy and to heat reaching the volume by convection or radiation must be balanced by the energy flux leaving the volume by surface re-radiation, heat conduction within solid and carried away by the produced mass which leaves the surface (blowing of ablative gases). As the surface mass and energy balances are mutually coupled, they must be solved jointly in an iterative way.

The surface mass balance (see Fig. 2) can be written as

$$\underbrace{\rho D \frac{\partial y_i}{\partial \eta}}_{\text{Diffusion}} + \underbrace{\dot{\omega}_i}_{\text{Chem. source}} = \underbrace{(\rho v)_w \cdot y_{i_w}}_{\text{Blowing}} \qquad (i = 1, \ldots, N) \tag{1}$$

A summation of Eq. 1 over all the species yields the total mass blowing flux

$$\sum_{i=1}^{N} \dot{\omega}_i = (\rho v)_w \qquad \Rightarrow \qquad \dot{m}_w = (\rho v)_w = \rho_s \cdot \dot{r} \tag{2}$$

where ρ_s represents the material density and $\dot{r}$ is the surface recession rate.

Multiplying Eq. 1 for each i species's enthalpy and summing over all the species yields an enthalpy balance from mass conservation

NUMERICAL ANALYSIS OF CATALYSIS AND ABLATION EFFECTS FOR CARBON-BASED ABLATIVE MATERIALS

$$\underbrace{\sum_{i=1}^{N} h_i \rho D \frac{\partial y_i}{\partial \eta}}_{\text{Diffusion heating}} + \underbrace{\sum_{i=1}^{N} h_i \dot{\omega}_i}_{\text{Heat release}} = \underbrace{\dot{m}_w h_w}_{\text{Blowing enthalpy}} \tag{3}$$

The surface energy balance (see Fig. 3) can be written as

$$\underbrace{k \frac{\partial T}{\partial \eta}}_{\text{Convective heating}} + \underbrace{\sum_{i=1}^{N} h_i \rho D \frac{\partial y_i}{\partial \eta}}_{\text{Enthalpy carried by diffusion}} + \underbrace{\dot{m}_w h_{s,w}}_{\text{Material enthalpy}} + \underbrace{q_{\text{rad}_{\text{in}}}}_{\text{Radiation in}} = \underbrace{q_{cw}}_{\text{Solid conduction}} + \underbrace{q_{\text{rad}_{\text{out}}}}_{\text{Radiation out}} + \underbrace{(\rho v)_w h_w}_{\text{Blowing}} \tag{4}$$

where h_w represents the enthalpy of the mixture of gases at the surface and $h_{s,w}$ represents the enthalpy of the solid material at the surface temperature.

Substituting Eq. 3 into Eq. 4 and neglecting radiation from the gas-phase yields

$$\underbrace{k \frac{\partial T}{\partial \eta}}_{\text{Convective heating}} \underbrace{- \sum_{i=1}^{N} h_i \dot{\omega}_i + \dot{m}_w h_{s,w}}_{\text{Heat flux of reaction}} = \underbrace{q_{cw}}_{\text{Solid conduction}} + \underbrace{q_{\text{rad}_{\text{out}}}}_{\text{Radiation out}} \tag{5}$$

by defining the heat of reaction as $\Delta h_{\text{reac}} = \left[\sum_{i=1}^{N} h_i (\dot{\omega}_i / \dot{m}_w) - h_{s,w} \right]$ and by assuming steady-state ablation so that the "heat conduction to solid" term can be expressed as $\dot{m}_w (h_{s,w} - h_{s,0})$ with $h_{s,0}$ representing the enthalpy of the solid material at its initial temperature, the final form of the energy balance equation is

$$\underbrace{k \frac{\partial T}{\partial \eta}}_{\text{Convective heating}} = \underbrace{\dot{m}_w \Delta h_{\text{reac}}}_{\text{Heat flux of reaction}} + \underbrace{\dot{m}_w (h_{s,w} - h_{s,0})}_{\text{Solid conduction (steady-state)}} + \underbrace{\sigma \epsilon T_w^4}_{\text{Re-radiation}} \tag{6}$$

where the solid material has been assumed as a grey body with surface emissivity equal to ϵ.

Nonequilibrium finite-rate GSI model (modified Park and Ahn)

The model reaction set contains irreversible **oxidation** (of both O and O_2), irreversible **nitridation** and **recombination** of N and reversible C_3 **sublimation**

Surface reaction	j	γ_j	E_j/R	reaction type	source
$C_s + O \rightarrow CO$	1	0.63	1160	Eley-Rideal	Park [1]
$2C_s + O_2 \rightarrow 2CO$	2	0.50	0	Eley-Rideal	Park [1]
$2N \rightarrow N_2$	3	0.03	0	Eley-Rideal	VKI [2]
$C_s + N \rightarrow CN$	4	8.441×10^{-3}	2322	Eley-Rideal	Suzuki [3]
$3C_s \leftrightarrow C_3$	5	5.19×10^{14}	90845	Sublimation	Park [1]

[1] Park et al., *Journal of Thermophysics and Heat Transfer*, 1999
[2] Turchi et al., *11th AIAA Thermophysics and Heat Transfer Conference*, 2014
[3] Suzuki et al., *Journal of Thermophysics and Heat Transfer*, 2010

Figure 4: Reference heterogeneous gas surface interaction model, from Refs.[13, 16, 19].

Finally, the chemical source terms due to the surface heterogeneous reactions, $\dot{\omega}_i$, are taken from the reference gas surface interaction model described in Fig. 4. The model includes five finite-rate reactions for: carbon oxidation by atomic oxygen, carbon oxidation by molecular oxygen, carbon nitridation by atomic nitrogen, carbon sublimation and atomic nitrogen recombination.

The carbon mass blowing rate contributions from the heterogeneous surface reactions with the atmospheric species (N, O and O_2) are expressed as

$$\dot{m}_i = k_j \rho_i \qquad (i = N, O, O_2) \tag{7}$$

where k_j is the effective rate constant for reaction j and ρ_i is the partial density of species i. The effective rate constant k_j can be expressed as

$$k_j = \left(\frac{\hat{v}_j}{4} \right) \cdot \underbrace{(\gamma_j) \cdot \exp(-E_j / RT_w)}_{\text{Effective reaction probability (or efficiency)}} \tag{8}$$

Test ID	Test gas	Mass flow rate	Pressure	Power
		g/s	hPa	kW
P-A-15-T1500	Air	18	16.5	85
P-A-15-T2000	Air	16	15	154
P-A-15-T2800	Air	16	15	343
P-A-250-T1500	Air	18	250	125
P-A-250-T2000	Air	16	250	174
P-A-250-T2800	Air	16	250	310
P-N-15-T1500	Nitrogen	18	16.5	114
P-N-15-T2000	Nitrogen	16	15	200
P-N-15-T2800	Nitrogen	16	15.6	410
P-N-250-T1500	Nitrogen	18	250	205
P-N-250-T2000	Nitrogen	16	250	264(256)
P-N-250-T2800	Nitrogen	16	250	338
A-A-15-T1500	Air	18	16.5	85
A-A-250-T2800	Air	16	250	319

Figure 5: Experimental test conditions (P = carbon preform;[15] A = ASTERM[14]).

where $\hat{v}_j$ represents the mean molecular speed of the reacting species

$$\hat{v}_j = \sqrt{8kT_w/\pi m_i} \qquad (9)$$

The carbon mass blowing rate contribution from the sublimation reaction (producing gaseous C_3) is expressed as

$$\dot{m}_i = k_j\rho(y_{i,eq} - y_i) \qquad (i = C_3) \qquad (10)$$

where $y_{i,eq}$ for species C_3 represents the equilibrium C_3 mass fraction that can be computed from its saturated equilibrium vapour pressure. The rate of production/consumption of the ith gas-phase species at the wall, $\dot{\omega}_i$, can be easily derived from the carbon mass blowing rates by the generic surface reaction, $\dot{m}_i$, and the mass balance available once the species molecular weights and the stoichiometry of the surface reactions are known (see Fig. 4).

From a numerical standpoint, the total ablation mass flux, $\dot{m}_w$, and the wall chemical composition, y_{i_w}, are computed from the surface mass balance, Eq. 1, coupled with the finite-rate ablation/catalysis model for $\dot{\omega}_i$ and using the local pressure and temperature distributions. The wall temperature, T_w, is computed from the surface energy balance, Eq. 6, using an iterative procedure to solve the highly non-linear coupling between the mass and energy balances. At each numerical iteration, the wall temperature, the ablation mass flux, and the wall chemical composition are updated until a steady-state condition is reached. This procedure has permitted to carry out all the computations presented in the next Sections without introducing any further numerical treatment to increase code robustness. Boundary conditions other than an ablating wall are enforced as follows: total temperature, total pressure, flow direction and chemical composition at the inflow (subsonic inflow), assigned static pressure at the outflow (subsonic outflow), and symmetry axis.

2.2 Carbon heterogeneous surface reaction kinetics

Before discussing the obtained results, a preliminary analysis of the carbon heterogeneous surface reaction kinetics and their associated heats of reaction is useful to understand their impact on the behavior of the thermal protection material for the analyzed test conditions.

Figure 5 presents a summary of the experimental test conditions and the test nomenclature. The initial attention will be devoted to nitrogen tests. The possible surface reactions that can take place at the carbon surface in a pure nitrogen environment are limited to: nitrogen recombination, carbon nitridation by atomic nitrogen attack and carbon sublimation. Carbon nitridation by atomic nitrogen attack is a heterogeneous surface reaction that has been receiving some noticeable attention lately due to recent experimental test (see, for example, Refs.[10, 13, 16, 19]). The more up-to-date data appear to be those from Suzuki et al.[?] and VKI experiments[10, 19] showing nitridation efficiency in the range 0.001 - 0.004. Based on the obtained efficiency values, Suzuki et al.[?] proposed a regression expression in the Arrhenius form as follows $\gamma_{nit} = 8.441 \cdot 10^{-3} \exp(-2322/T)$. Concerning atomic nitrogen recombination at

NUMERICAL ANALYSIS OF CATALYSIS AND ABLATION EFFECTS FOR CARBON-BASED ABLATIVE MATERIALS

(a) Surface reaction efficiency vs temperature

(b) Heat of reaction vs temperature
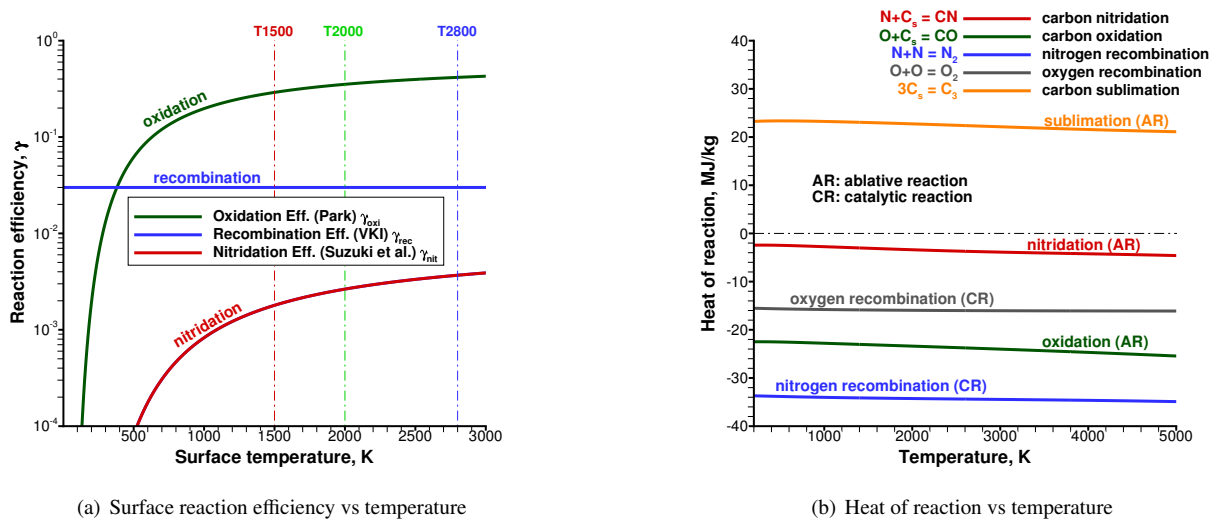
Figure 6: Reaction efficiency and heat of reaction of air/carbon reactions.

a carbon surface, recent VKI data shows recombination efficiencies in the range 0.03 - 0.035. Figure 6(a) plots the surface reaction efficiencies vs temperature showing that the probability of nitrogen recombination is 10 to 15 times higher than that of nitridation in the temperature range of interest (from 1500 to 2800 K). Figure 6(b) shows the heat of reaction as a function of temperature for the surface reactions showing that nitridation heat of reaction is only a small fraction ($\approx 10\%$) of the nitrogen recombination heat of reaction (both are exothermic reactions). For what concerns the sublimation process, it is strongly endothermic and is dependent upon both pressure and temperature. Figure 7 shows the C_3 equilibrium vapour pressure vs temperature. The sublimation temperature is dependent upon pressure and is close to 3500 K (at stagnation point) for all of the low pressure cases (at 15 mbar). As sublimation is driven by $\left(p_{C_3,eq} - p_{C_3}\right)$ it becomes important only when the vapour pressure is not negligible with respect to the external pressure. As Fig. 7 clearly shows, P-N-15-T2800 is the only case where sublimation may have a role.
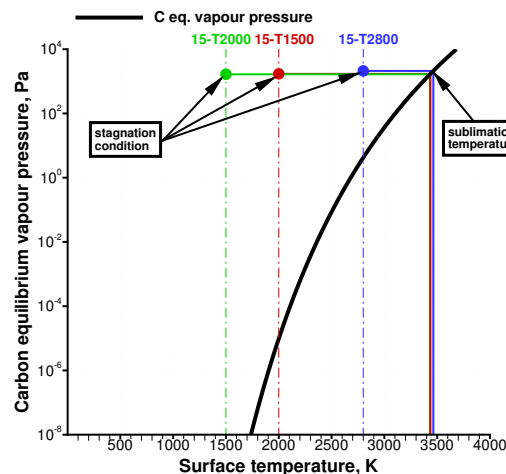
Figure 7: C_3 equilibrium vapour pressure vs temperature.

For air cases, two other surface reactions have to be included: oxygen recombination and carbon oxidation by atomic oxygen attack. The carbon oxidation surface by molecular oxygen attack, although included in the reference gas surface interaction model (see Fig. 4), is not relevant for the present study as molecular oxygen concentration has been shown to be negligibly small for all of the experimental test condition that have been analyzed. Figure 6(a) shows the nitridation, recombination and oxidation reaction efficiency vs temperature showing that the probability of carbon oxidation is one order of magnitude higher than that of carbon nitridation in the temperature range of interest (from 1500 to 2800 K). Therefore, it is expected that, for air cases, most of the mass loss will be due to oxidation

NUMERICAL ANALYSIS OF CATALYSIS AND ABLATION EFFECTS FOR CARBON-BASED ABLATIVE MATERIALS
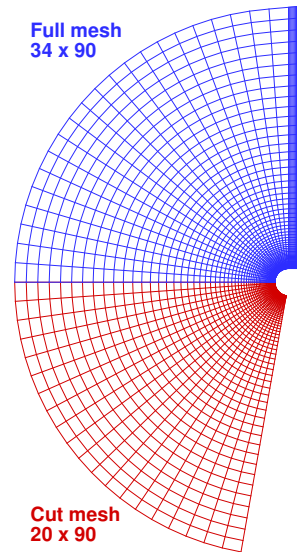
Figure 8: Flow analysis full grid (top) and "cut-out" grid (bottom).

rather than nitridation. Concerning the oxygen recombination reaction efficiency, it is not shown in Fig. 6(a) nor it is present in the reference gas surface interaction model, as there is no experimental evidence in the open literature of atomic oxygen recombining over a carbon surface. This is expected to be related to the large reaction probability of the carbon oxidation reaction, dominating over any other surface reaction involving atomic oxygen consumption. Finally, Fig, 6(b) shows the heat of reaction as a function of temperature for all of the five above discussed surface reactions. The sublimation reaction is the sole endothermic reaction. Among the other exothermic reactions, the larger heat of reaction is associated to nitrogen recombination followed by carbon oxidation, $\approx 30\%$ smaller, with a negligibly small contribution coming from carbon nitridation, as previously noted.

3. Results and discussion

This part contains results from the CFD calculations conducted for carbon preform samples in pure nitrogen and air environments. The first objective of this work has been to investigate the ablation (i.e. surface nitridation, oxidation, and sublimation, if any) and catalysis (i.e. nitrogen recombination) behavior of the sample as a function of surface conditions in two different environments in order to identify the model parameters that are mostly affecting the predictions. The performed calculations have been compared to available measured data from the experiments. The second objective has been the set-up of an "inverse approach" that is used to extract the effective reaction probabilities from both numerical simulations and experimental data.

It is worth noting that the stagnation point of the carbon preform sample has received special attention during this study as most of the measured data have been collected at this point. Finally, the numerical convergence was good for all of the low-pressure cases (see Figure 5), at 15 mbar, although the number of iterations required to achieve convergence increased as the inflow Mach number decreased. However, due to the significantly lower Mach number of the high-pressure cases (as low as 0.01), at 250 mbar, significant convergence issues have arisen. Hence, the numerical rebuilding has been focused only on the low-pressure test cases.

3.1 Flow field analysis

Due to the significant number of expected simulations, the numerical grids have to be carefully selected in order to provide good accuracy of the results but at the same time to allow efficient parametric analysis at an affordable computational cost. Figure 8 presents the grid which has been used to perform the flowfield calculations for the carbon preform samples in pure nitrogen environment. The computational domain is subdivided into 34 x 90 grid points in the azimuthal and radial directions, respectively. The grid starts at 20 x R (radius) upstream of the sample stagnation point to accurately describe the upstream subsonic flowfield. The inflow conditions, total temperature, total pressure, flow direction and chemical composition were assigned to the left hand side of the analysis grid while subsonic outflow was assigned to the right hand side.

(a) Pressure flowfield with full grid (top) and "cut-out" grid (bottom)

(b) Surface pressure and temperature distributions
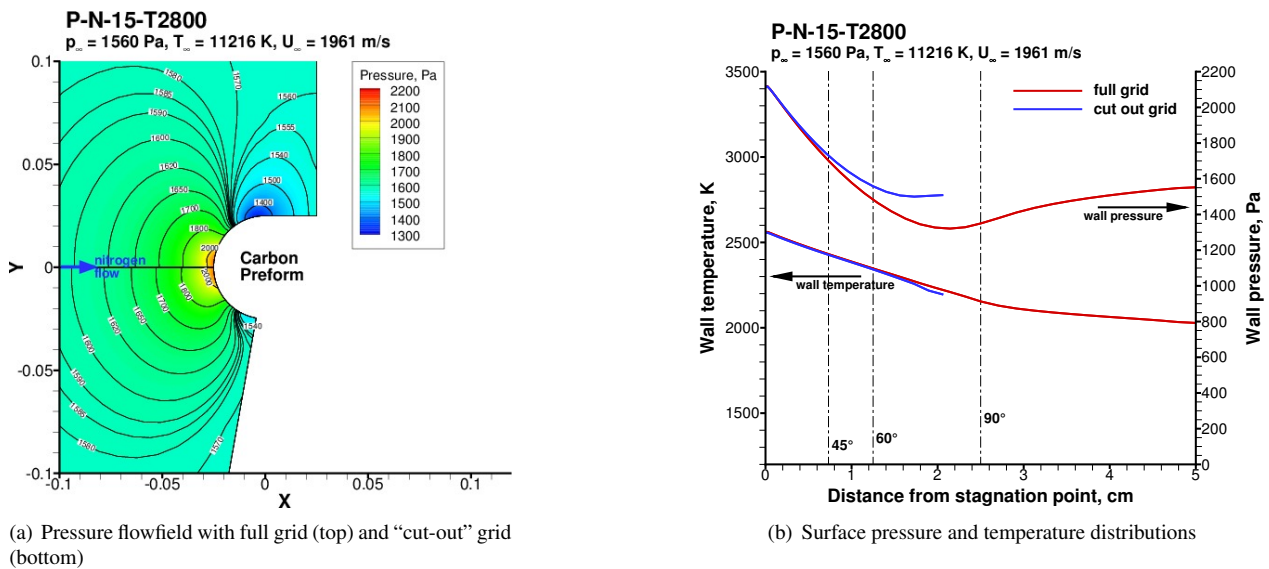
Figure 9: Pressure distributions with full and "cut-out" grid.

A second analysis grid, also shown in Fig. 8, was developed to calculate the flowfield only in the stagnation point region of the sample, to focus on the ablation/catalysis processes on this region and save computational time. This grid, subdivided into 20 x 90 grid points in the azimuthal and radial directions, is referred to as the "cut-out" grid since it is terminated just before the conical part of the sample (from stagnation up to 80°). A comparison of results from the complete grid and the "cut-out" grid are shown in Fig. 9, for a reference condition at a static pressure of 1560 Pa. As it can be clearly seen, the results in the stagnation point region are identical for both grids and they start to diverge from each other starting at 45° from stagnation point and downstream. Therefore, the "cut-out" can be considered sufficiently accurate when a description of the sole stagnation point region is needed. However, the full grid is the reference grid and it will be used from now on. The "cut-out" grid is used only when explicitly specified in the text. Note that all the computations presented here are at the steady-state condition obtained by iterating in time until residuals drop by at least five orders of magnitude. The CFD solution has been verified by a grid convergence analysis on three grid levels. The finest mesh has 68 x 180 cells in the azimuthal and radial direction, respectively. Each mesh coarsening is made by removing one node out of two in each coordinate direction. The quantitative analysis of solutions obtained on three grid levels confirms that the spatial order of accuracy is, in most region of the flowfield, close to the formal second-order value of the scheme. This confirms the asymptotic behavior of the numerical error, and thus gives a good confidence on the error estimate. The discrepancy between the surface quantities (temperature, pressure, ablation mass flux, etc.) evaluated with the medium and fine grids is less than 1% at the stagnation point location and less than 3% elsewhere; therefore, the medium grid has been considered sufficiently refined for the present analysis.

Flowfield results from the calculations performed for test cases P-N-15-T2000 and P-A-15-T2000 are shown in Figs. 10 and 11 that show both temperature and pressure contours. As shown, the reference grid is sufficiently large to have practically undisturbed flow condition at inflow which ensures that the upstream subsonic flowfield is accurately solved for both nitrogen and air test cases.

Flowfield results in terms of chemical species are shown in Figs. 12 and 13 for the nitrogen test cases P-N-15-T1500 and P-N-15-T2800 and in Figs. 14, 15, and 16 for the air test cases P-A-15-T1500 and P-A-15-T2800. Figure 12 shows the species N and N_2 contours over the domain. For P-N-15-T2800, due to the higher freestream temperature, the freestream composition is almost entirely composed by atomic nitrogen. Differently, for P-N-15-T1500, there is a significant amount of molecular nitrogen in the freestream. As shown, due to the surface catalycity, atomic nitrogen is recombining at the surface. The N_2 mass fraction always peaks at the surface, with the highest values that are reached in the conical part of the sample.

Figure 13 shows the species CN and C_3 contours over the domain. The species CN is the product of carbon nitridation while the species C_3 is the product of carbon sublimation. As shown, carbon nitridation is active everywhere at the surface while carbon sublimation is only visible in the stagnation point region. Moreover, C_3 is present in a non-negligible amount in the stagnation region only for P-N-15-T2800. The mass fraction of CN produced at the surface is lowest for P-N-15-T1500 and highest for P-N-15-T2800.

Figure 14 shows the species N and N_2 contours over the domain for air environment. As for pure nitrogen test cases, due to the surface catalycity, atomic nitrogen is recombining at the surface. The N_2 mass fraction always peaks

NUMERICAL ANALYSIS OF CATALYSIS AND ABLATION EFFECTS FOR CARBON-BASED ABLATIVE MATERIALS

(a) Pressure (top) and temperature (bottom) flowfields over the domain

(b) Pressure (top) and temperature (bottom) flowfields close to sample
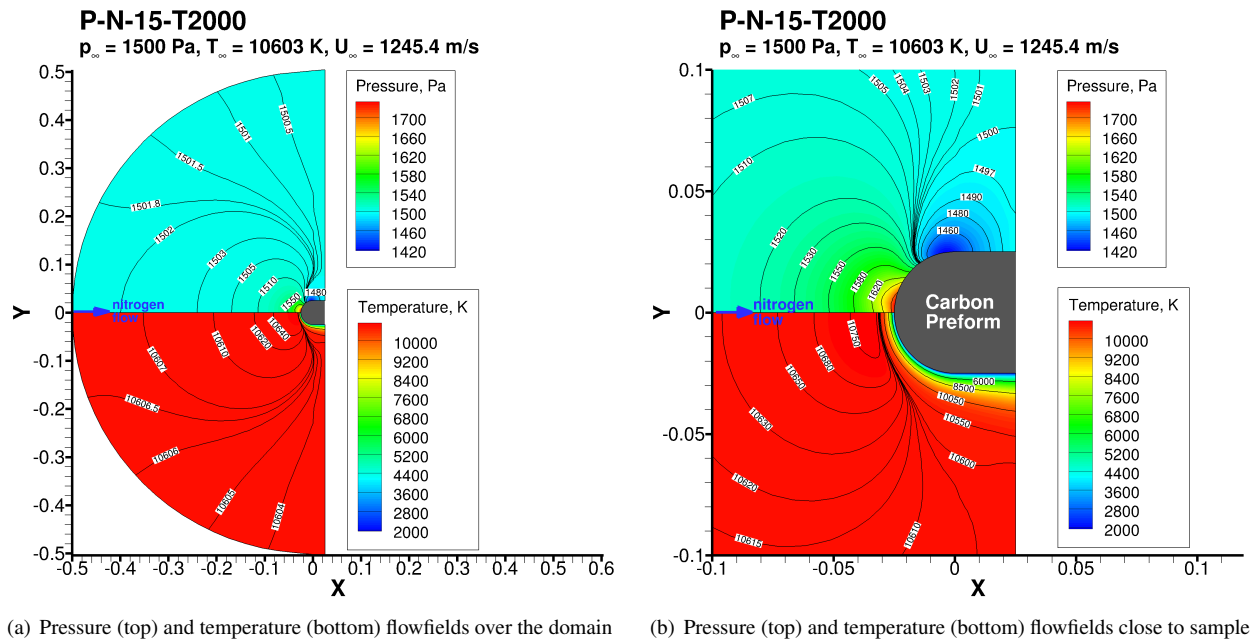
Figure 10: Flowfields for P-N-15-T2000 nitrogen test case.

(a) Pressure (top) and temperature (bottom) flowfields over the domain

(b) Pressure (top) and temperature (bottom) flowfields close to sample
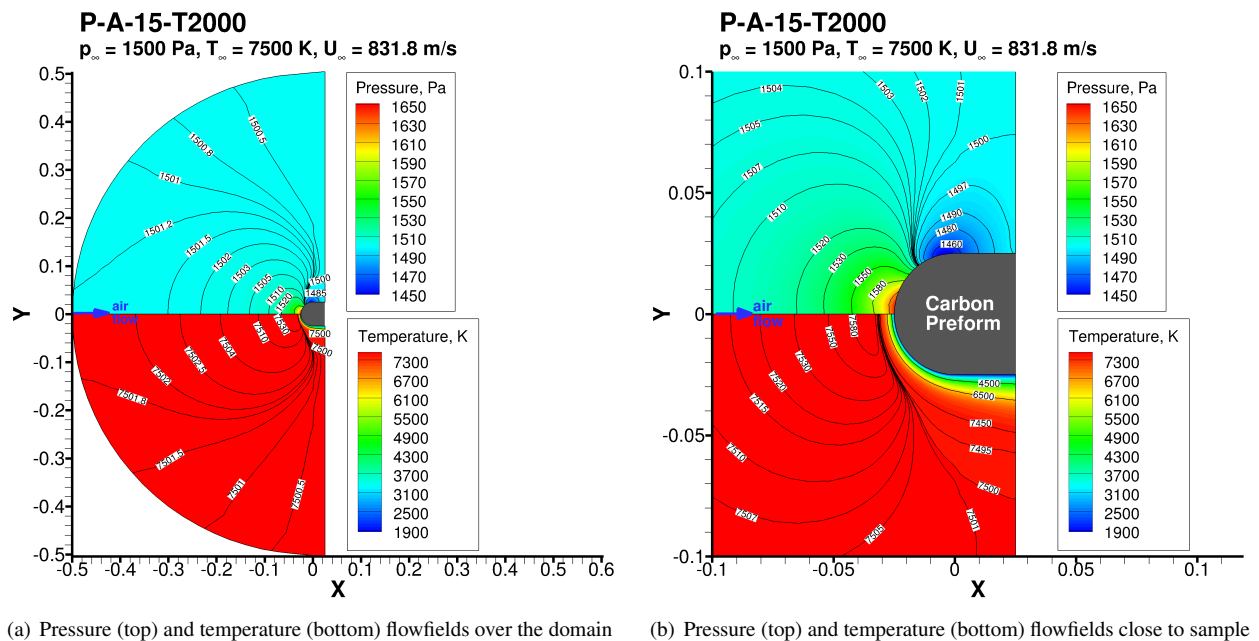
Figure 11: Flowfields for P-A-15-T2000 air test case.

at the surface, with the highest values that are reached in the conical part of the sample for all test cases, as already noted for the pure nitrogen tests.

Figure 15 shows the species CN and C_3 contours over the domain for air environment. As shown, carbon nitridation is active everywhere at the surface while carbon sublimation is only visible in the stagnation point region. Moreover, as for pure nitrogen tests, C_3 mass fraction at the surface is vanishing small, denoting that sublimation is practically negligible. The mass fraction of CN produced at the surface is lowest for P-A-15-T1500 and highest for P-A-15-T2800, as for pure nitrogen tests. However, differently from the nitrogen tests where CN was monotonically decreasing with increasing distance from the surface, CN in air tests is shown to exhibit a local peak inside the boundary layer that is clearly visible for P-A-15-T2800.

Finally, Fig. 16 shows the species CO and O contours over the domain for air environment. It is worth noting that, differently from molecular nitrogen that is not fully dissociated for P-A-15-T1500 (as for P-N-15-T1500), due to

NUMERICAL ANALYSIS OF CATALYSIS AND ABLATION EFFECTS FOR CARBON-BASED ABLATIVE MATERIALS

(a) P-N-15-T1500 test case

(b) P-N-15-T2800 test case
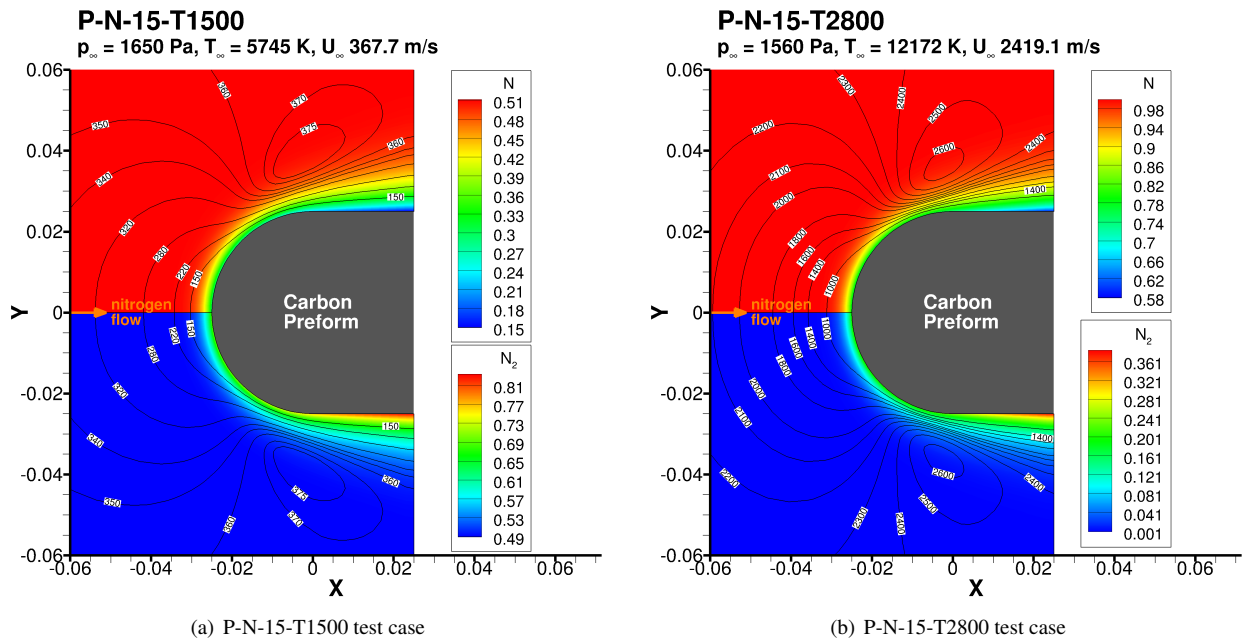
Figure 12: Flowfields for N (top) and N_2 (bottom) over the domain for nitrogen test cases.

(a) P-N-15-T1500 test case

(b) P-N-15-T2800 test case
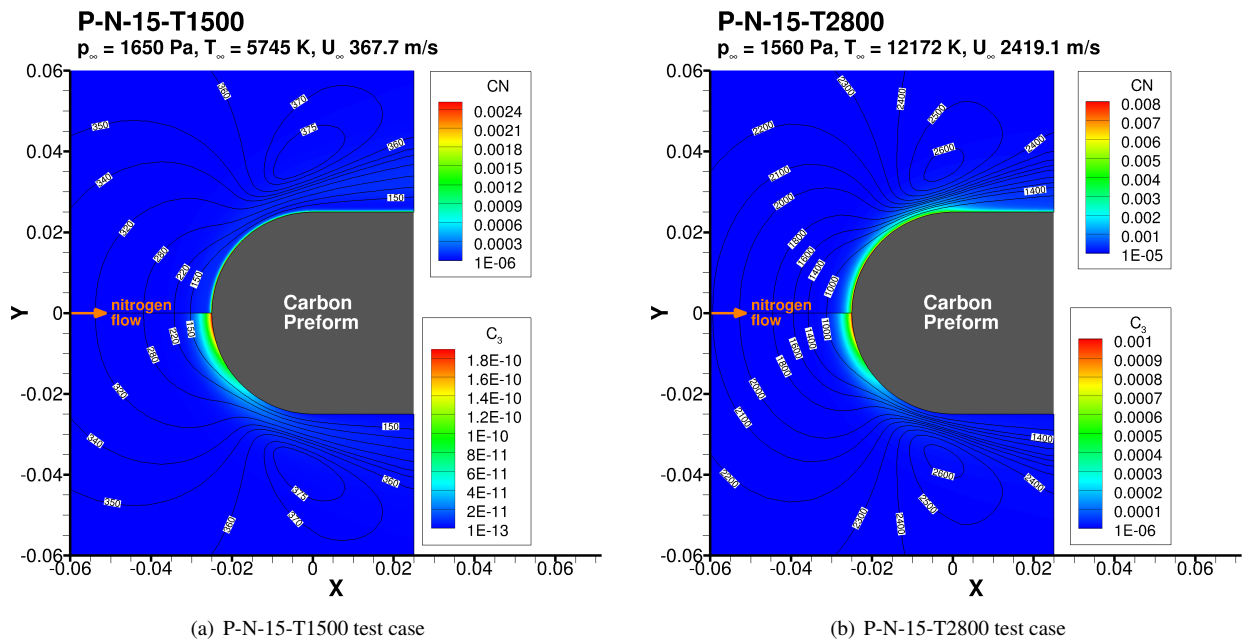
Figure 13: Flowfields for CN (top) and C_3 (bottom) over the domain for nitrogen test cases.

the lower freestream temperature, the freestream composition is entirely composed by dissociated oxygen for all air cases. Hence, no molecular oxygen is available in the freestream for any test. The species CO is the product of carbon oxidation and it is shown to be active everywhere at the surface. As carbon monoxide is produced at the expense of atomic oxygen, the mass fraction of O appears to be negligibly small at the surface, especially in the conical part, denoting an almost diffusion-limited regime. Differently from the pure nitrogen cases, where the nitridation product CN was representing only a small part of the gaseous mixture in the boundary layer, carbon monoxide represent $\approx 30\%$ by mass of the boundary layer mixture.

NUMERICAL ANALYSIS OF CATALYSIS AND ABLATION EFFECTS FOR CARBON-BASED ABLATIVE MATERIALS

(a) P-N-15-T1500 test case

(b) P-N-15-T2800 test case
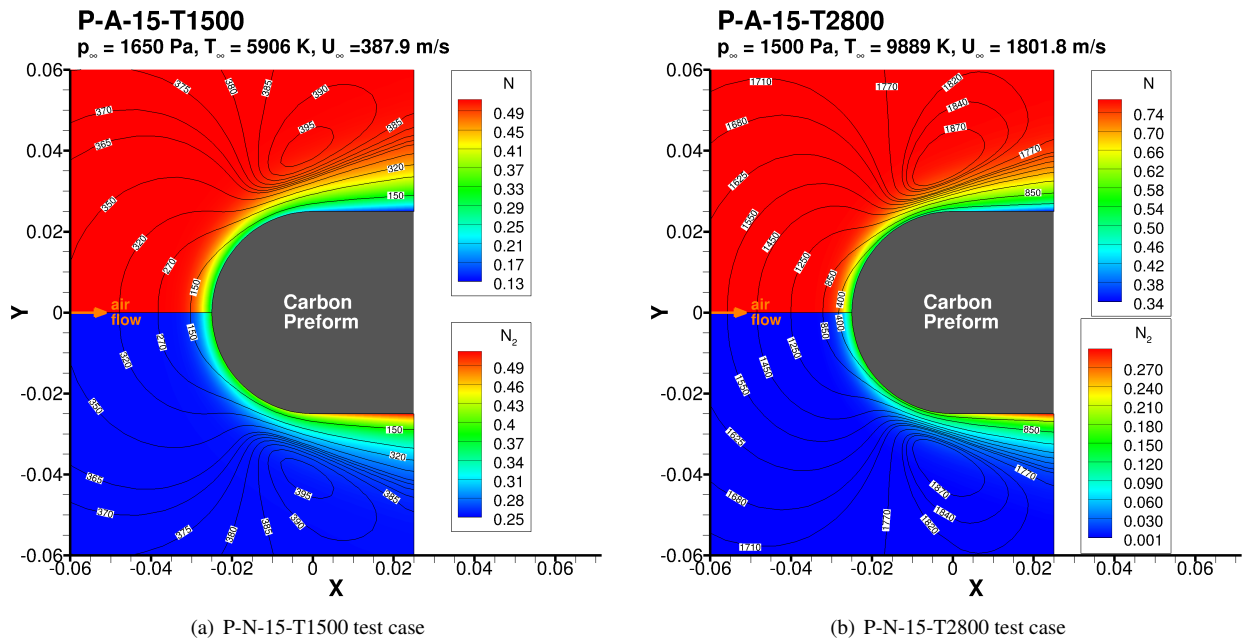
Figure 14: Flowfields for N (top) and N_2 (bottom) over the domain for air test cases.

(a) P-N-15-T1500 test case

(b) P-N-15-T2800 test case
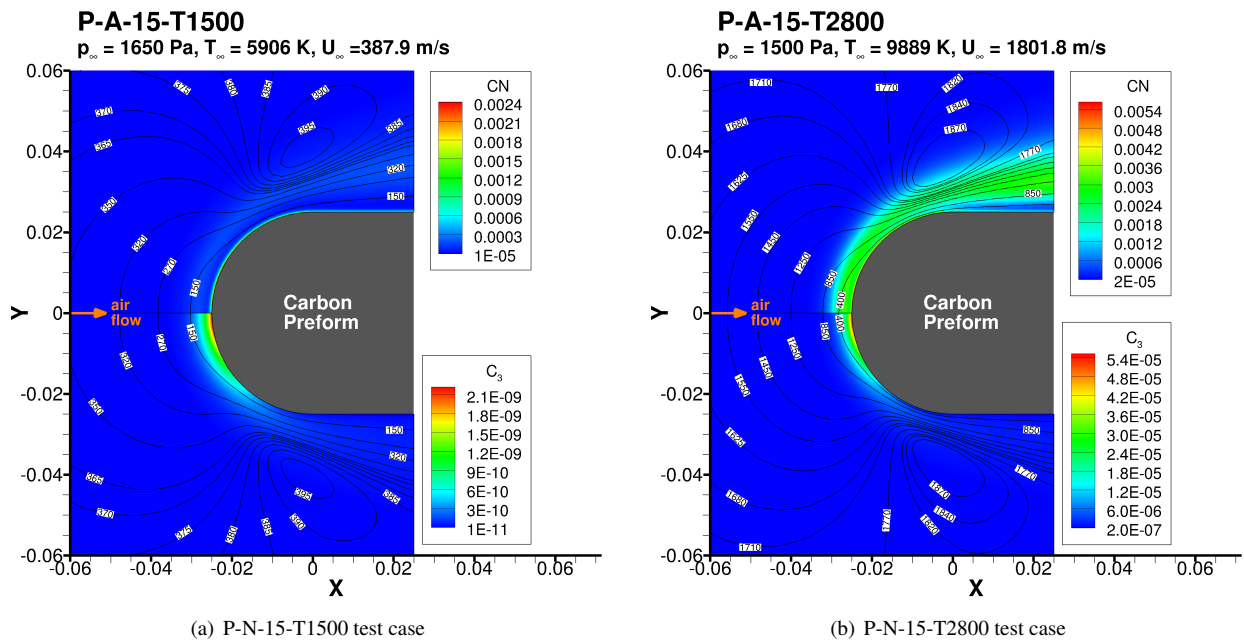
Figure 15: Flowfields for CN (top) and C_3 (bottom) over the domain for air test cases.

3.2 Comparison with surface measurements

The distributions of mass blowing flux and temperature along the carbon preform surface are shown in Fig. 17 for nitrogen tests along with the experimental measurements taken at the stagnation point. Numerical results have been obtained from the solution of the surface mass and energy balances using the reference gas surface interaction model and assuming a surface emissivity of 0.9. It can be seen that both the ablation mass flux, $\dot{m}$, and the surface temperature, T_w, distributions are quite flat, especially at the lower T_w. This is also confirmed by the experimentally measured shape history of the tested samples, that shows a quite uniform ablation all along the spherical shape. Fig. 17(a) also reports the different contributions from nitridation and sublimation, showing that the sublimation contribution to $\dot{m}$ is practically negligible for the lower temperature cases, P-N-15-T1500 and P-N-15-T2000, and it only represents 5% of the total ablation mass flux for the highest temperature case, P-N-15-T2800.

(a) P-N-15-T1500 test case

(b) P-N-15-T2800 test case
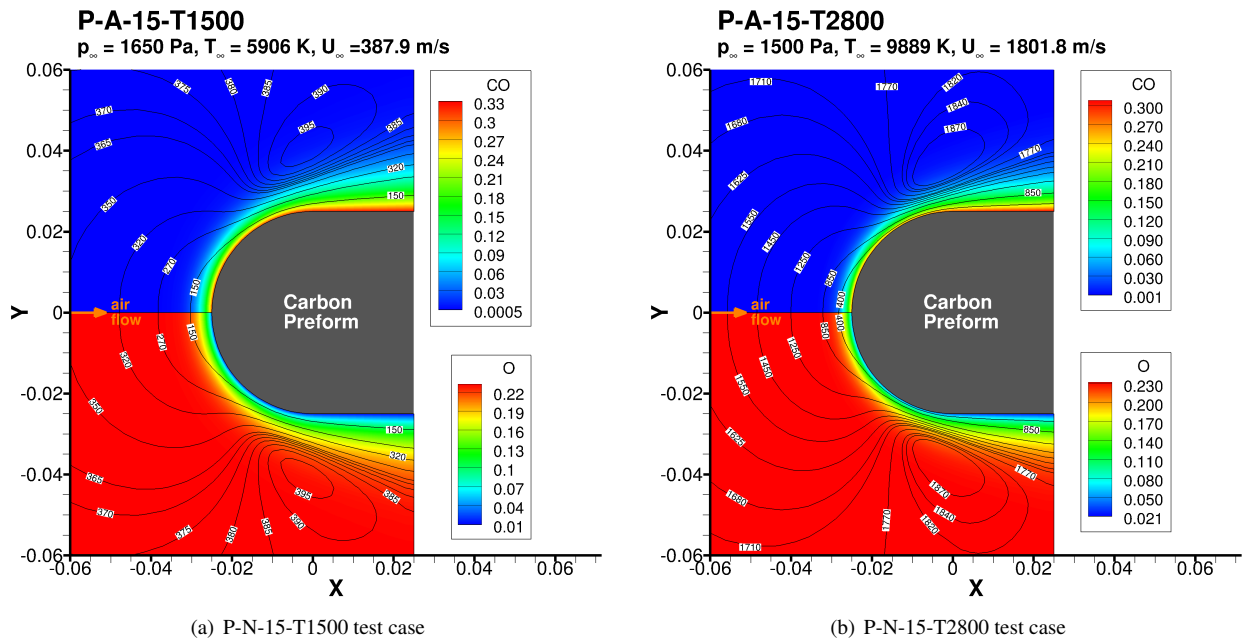
Figure 16: Flowfields for CO (top) and O (bottom) over the domain for air test cases.

(a) Mass blowing flux for the three test conditions

(b) Surface temperature for the three test conditions
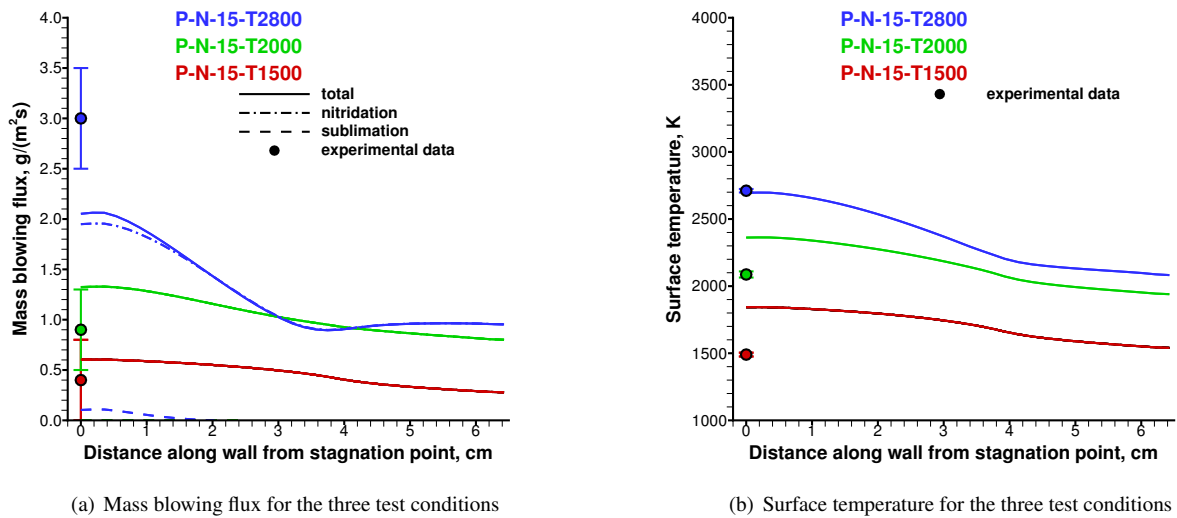
Figure 17: Distributions of mass blowing flux and temperature along the sample surface for nitrogen test cases.

Comparison with experimental measurements shows that $\dot{m}$ is within the experimental measurements error for P-N-15-T1500 and P-N-15-T2000, and it is underestimated by 32% for P-N-15-T2800, which shows an experimental error of ±17%. Looking at Fig. 17(b), surface temperature is within the experimental error for P-N-15-T2800 and is outside the experimental error for P-N-15-T2000 (+13%) and for P-N-15-T1500 (+24%). The numerical simulations that have been performed for carbon preform in pure nitrogen environment confirmed that carbon sample recession for the experimental test cases is dominated by nitridation, as carbon sublimation is practically not activated. The obtained results with the reference gas surface interaction model can be considered sufficiently satisfactory as they are able to correctly reproduce the qualitative behavior of the tests with maximum quantitative errors of about ±30% on the measured quantities $\dot{m}$ and T_w.

As far as the air test cases are concerned, the distributions of mass blowing flux and temperature along the carbon preform surface are shown in Fig. 18 along with the experimental measurements taken at the stagnation point. Both the ablation mass flux and the surface temperature distributions are quite flat, even though slightly less than what experienced for pure nitrogen tests. Fig. 18(a) also reports the different contributions from oxidation and nitridation,

NUMERICAL ANALYSIS OF CATALYSIS AND ABLATION EFFECTS FOR CARBON-BASED ABLATIVE MATERIALS

(a) Mass blowing flux for the three test conditions

(b) Surface temperature for the three test conditions
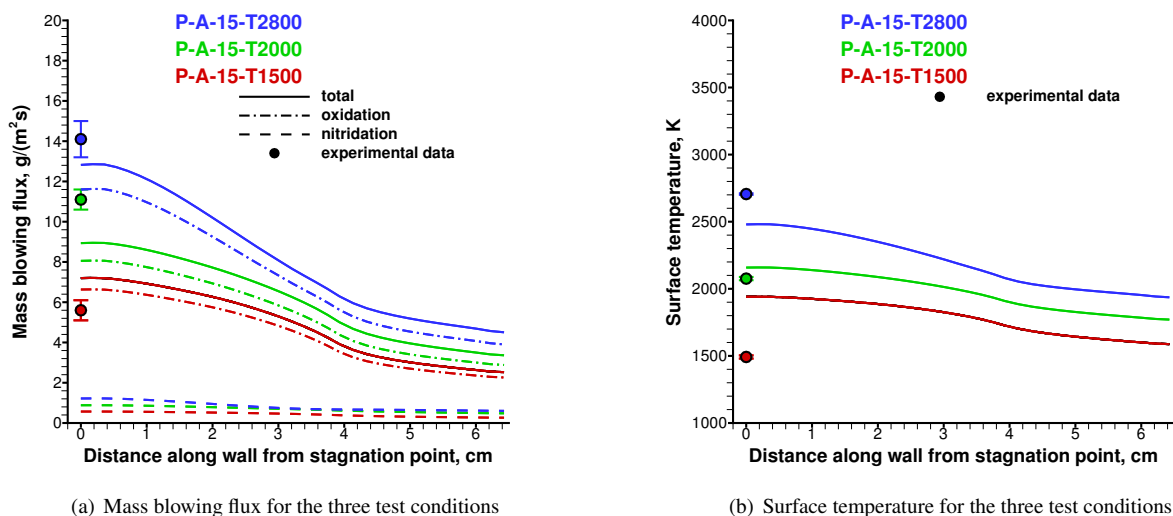
Figure 18: Distributions of mass blowing flux and temperature along the sample surface for air test cases.

showing that the oxidation contribution to $\dot{m}$ is dominant, with nitridation representing roughly 10% of the total ablation mass flux for the three test cases. Comparison with experimental measurements shows that $\dot{m}$ is almost within the experimental measurements error (lower bound) for P-A-15-T2800 and it is underestimated by 19% for P-A-15-T2000 and overestimated by 28% for P-A-15-T2000. Surface temperature, as shown in Fig. 18(b), is underestimated by 8% for P-A-15-T2800 and overestimated by 4% and 30% for P-A-15-T2000 and P-A-15-T1500, respectively. The numerical simulations that have been performed for carbon preform in air environment confirmed that carbon sample recession for the experimental test cases is dominated primarily by oxidation (contributing to roughly 90% of the recession rate) and secondarily by nitridation (contributing to roughly 10% of the recession rate), as carbon sublimation is practically not activated. As discussed for pure nitrogen cases, the obtained results with the reference gas surface interaction model for air tests can be considered sufficiently satisfactory as they are able to correctly reproduce the qualitative behavior of the tests with maximum quantitative errors of about ±30% on the measured quantities $\dot{m}$ and T_w.

3.3 Sensitivity analysis

A thorough sensitivity analysis to several parameters that can influence the sample ablation/catalysis process has been performed for the three low pressure cases for both pure nitrogen and air environments. For pure nitrogen tests, the analyzed parameters included: Schmidt number, surface emissivity, nitrogen recombination efficiency, and carbon nitridation efficiency.

The distributions of mass blowing flux and temperature along the sample surface for varying Schmidt number are shown in Fig. 19. The Schmidt number is mildly affecting the mass blowing flux as carbon nitridation reaction is limited by chemical kinetics rather than by atomic nitrogen diffusion. Therefore, the effect of the Schmidt number on carbon mass blowing flux is small, with ±8% for P-N-15-T1500 and ±4% for P-N-15-T2000 and P-N-15-T2800, due to the higher availability of atomic nitrogen at the surface for the latter cases, as shown in Fig. 12. The effect of the Schmidt number on the surface temperature is negligible, as shown in Fig. 19(b), as the effect on the mass blowing flux is limited; furthermore, the heat of reaction associated with the nitridation reaction has been shown to be small. In conclusion, the Schmidt number cannot be responsible for the surface temperature overestimation for P-N-15-T1500 and P-N-15-T2000.

The distributions of mass blowing flux and temperature along the sample surface for varying surface emissivity are shown in Fig. 20. The surface emissivity is only affecting the mass blowing flux at the highest surface temperature, for P-N-15-T2800, due to the activation of the sublimation reaction. Apart from this effect on the carbon sublimation reaction, surface emissivity is practically not affecting the mass blowing flux owing to carbon nitridation. Differently, the effect of the the surface emissivity on the surface temperature is significant for all of the three cases, as shown in Fig. 20(b), as the emissivity is directly affecting the surface energy balance. The higher the surface emissivity, the lower the surface temperature. However, even considering surface emissivities as high as 1.0, the surface temperatures for P-N-15-T1500 and P-N-15-T2000 still result to be overestimated.

The distributions of mass blowing flux and temperature along the sample surface for varying recombination

13

NUMERICAL ANALYSIS OF CATALYSIS AND ABLATION EFFECTS FOR CARBON-BASED ABLATIVE MATERIALS

(a) Mass blowing flux for the three test conditions

(b) Surface temperature for the three test conditions
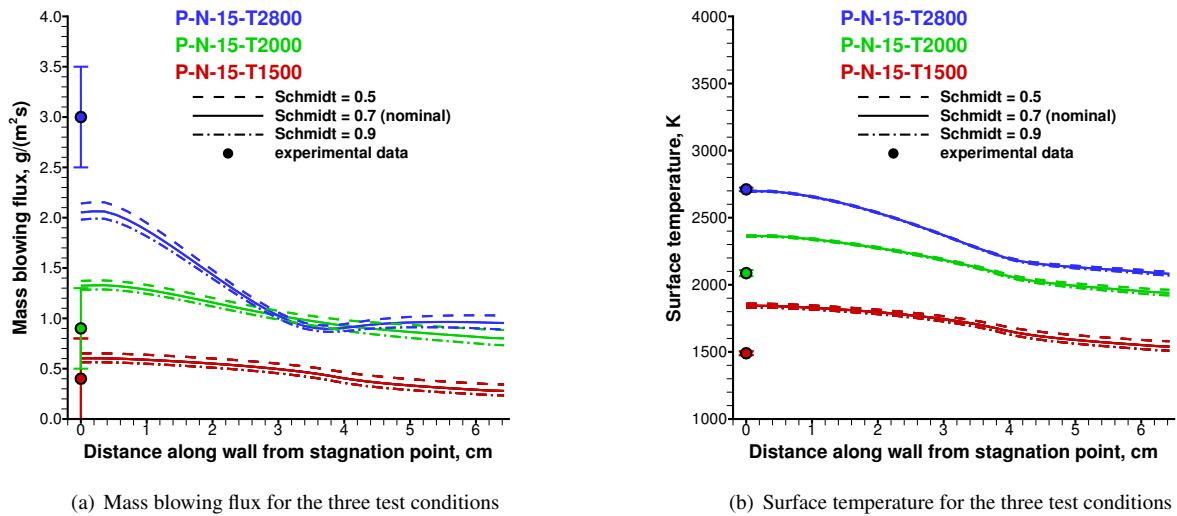
Figure 19: Distributions of mass blowing flux and temperature along the surface for varying Schmidt number.

(a) Mass blowing flux for the three test conditions

(b) Surface temperature for the three test conditions
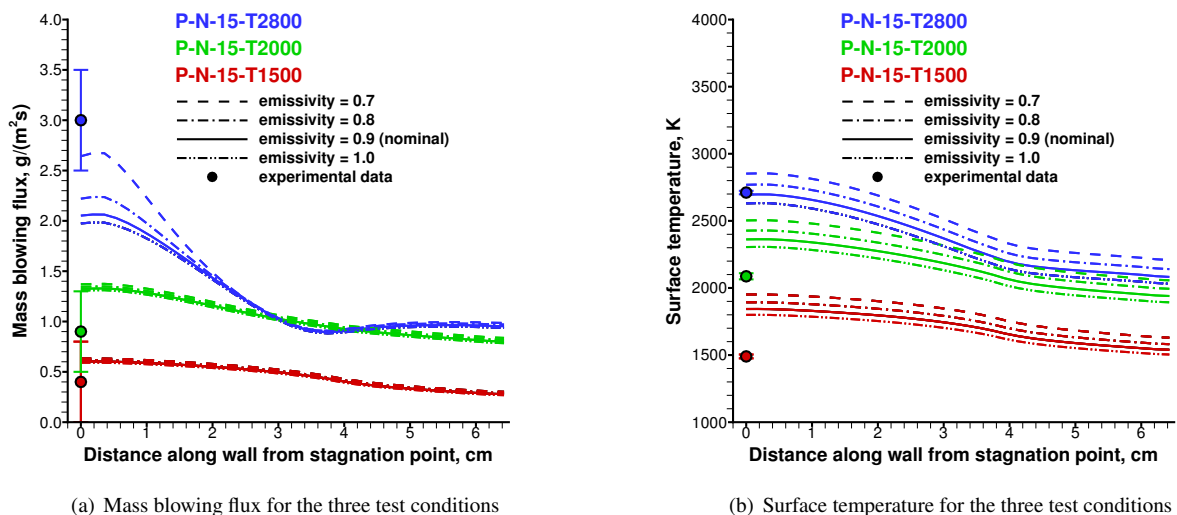
Figure 20: Distributions of mass blowing flux and temperature along the surface for varying surface emissivity.

efficiency (γ_{rec}) are shown in Fig. 21. Nitrogen recombination efficiency is affecting both the mass blowing flux, Fig. 21(a), and the surface temperature, Fig. 21(b). The surface temperature is directly influenced by the recombination efficiency because of the associated significant heat of recombination: the higher the recombination efficiency, the higher the surface temperature. Computed results show that for null recombination efficiencies the overestimation of surface temperatures for P-N-15-T1500 and P-N-15-T2000 drops significantly passing from +24% and +13% to +5% and +3%, respectively. The effect of the recombination efficiency on the mass blowing flux, as shown in Fig. 21(a), is, on the other hand, indirect: the higher the recombination efficiency, the lower the availability of atomic nitrogen at the surface. With less atomic nitrogen available at the surface, the carbon nitridation reaction effectiveness is reduced. Therefore, Fig. 21 clearly shows the competition between recombination reaction and nitridation reaction, as both are consuming atomic nitrogen and hence are affecting one another. The latter reaction (nitridation) is mainly affecting the mass blowing flux with negligible effect on the surface temperature, due to its reduced heat of reaction, as it will be later shown; the former reaction (recombination) does not strongly affect the mass blowing flux while it can significantly affect the surface temperature.

Finally, the distributions of mass blowing flux and temperature along the sample surface for varying nitridation efficiency (γ_{nit}) are shown in Fig. 22. Carbon nitridation efficiency is significantly affecting the mass blowing flux,

NUMERICAL ANALYSIS OF CATALYSIS AND ABLATION EFFECTS FOR CARBON-BASED ABLATIVE MATERIALS

(a) Mass blowing flux for the three test conditions

(b) Surface temperature for the three test conditions
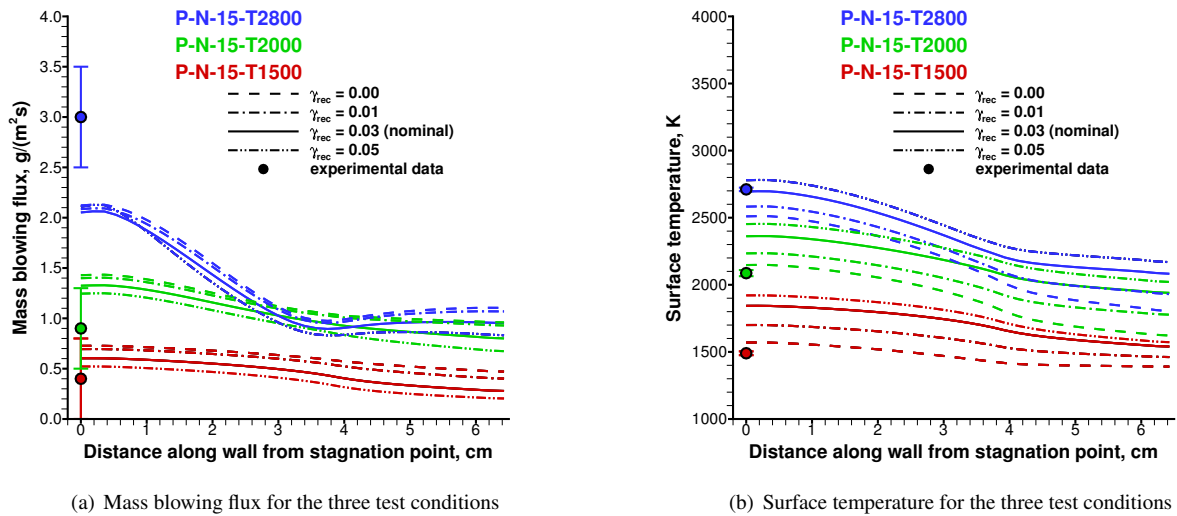
Figure 21: Distributions of mass blowing flux and temperature along the surface for varying recombination efficiency.

(a) Mass blowing flux for the three test conditions

(b) Surface temperature for the three test conditions
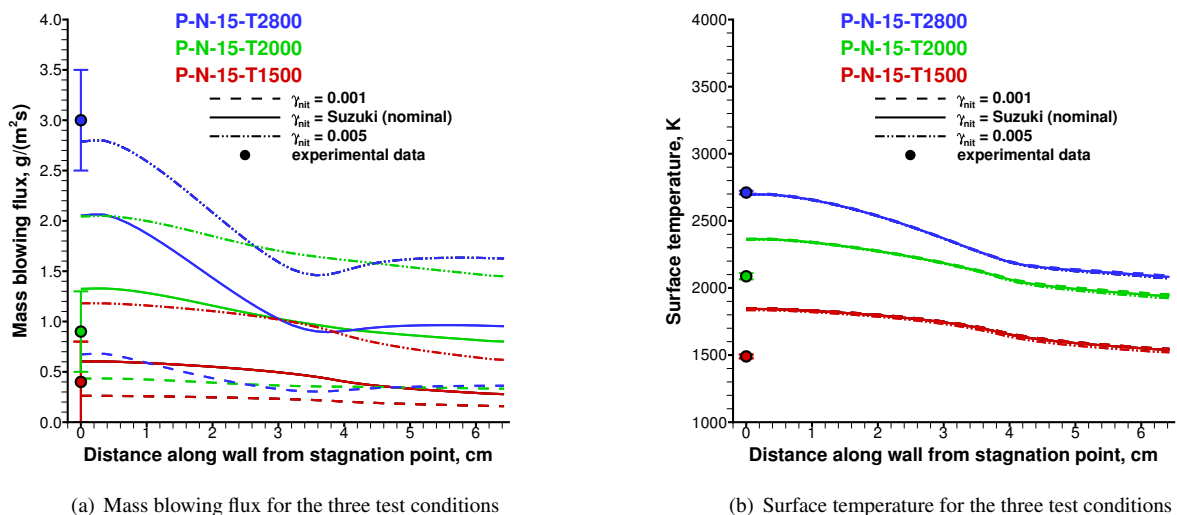
Figure 22: Distributions of mass blowing flux and temperature along the surface for varying nitridation efficiency.

Fig. 22(a), while it is practically not affecting the surface temperature, Fig. 22(b). The mass blowing flux is obviously directly influenced by the nitridation efficiency: the higher the nitridation efficiency, the higher the mass blowing flux. Differently, the surface temperature is practically not influenced by the nitridation reaction because of the small heat of reaction associated with the carbon nitridation. The thorough sensitivity analysis that has been performed for pure nitrogen tests revealed that the surface temperature is primarily affected by the recombination efficiency and secondarily by the surface emissivity. On the other hand, the surface recession is primarily affected by the nitridation efficiency, secondarily by the recombination efficiency (as it reduces the amount of available N atoms at the surface) that is competing with nitridation, and only tertiary by the Schmidt number. Moreover, the sensitivity analysis also confirmed that the nitridation efficiency has no impact on the wall temperature.

For air tests, the analyzed parameters included: Schmidt number, surface emissivity, nitrogen recombination efficiency, carbon oxidation efficiency, and carbon nitridation efficiency. The distributions of mass blowing flux and temperature along the sample surface for varying Schmidt number are shown in Fig. 23. The Schmidt number is quite evidently affecting the mass blowing flux, as carbon oxidation reaction has been shown to be limited mostly by atomic oxygen diffusion rather than by its chemical kinetics. Therefore, the effect of the Schmidt number on carbon mass blowing flux is quite significant, with ±19% for P-A-15-T1500, ±18% for P-A-15-T2000 and ±17% P-A-15-T2800,

NUMERICAL ANALYSIS OF CATALYSIS AND ABLATION EFFECTS FOR CARBON-BASED ABLATIVE MATERIALS

(a) Mass blowing flux for the three test conditions

(b) Surface temperature for the three test conditions
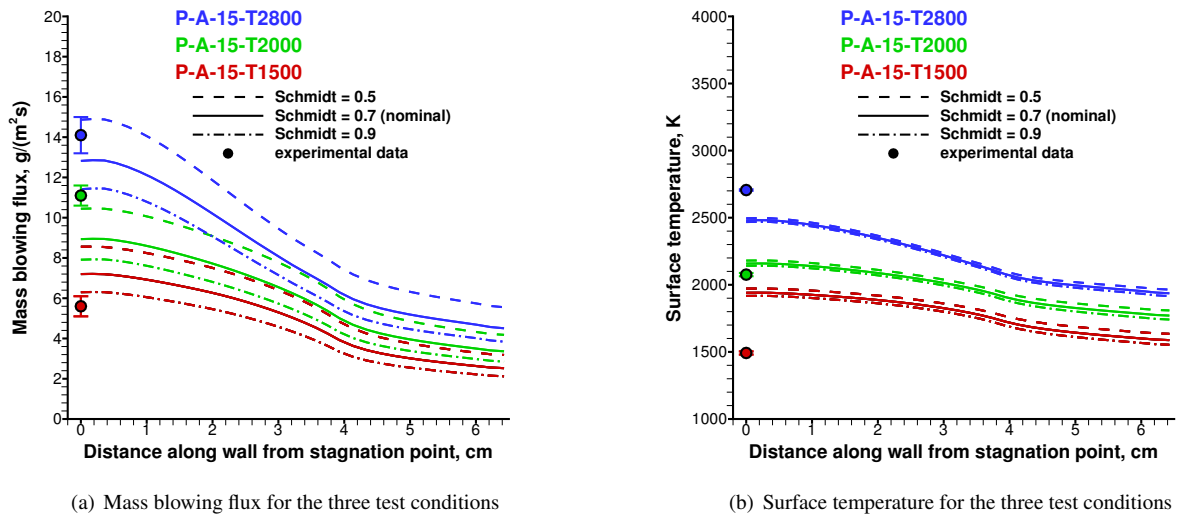
Figure 23: Distributions of mass blowing flux and temperature along the surface for varying Schmidt number.

due to the slightly higher availability of atomic oxygen at the surface for the latter cases, as shown in Fig. 16. The effect of the Schmidt number on the surface temperature is very limited, as shown in Fig. 23(b), as experienced for the nitrogen cases. However, in this case, the reason is different as the heat release associated with the oxidation reaction is significant and one would expect an increase of surface temperature with an increase of mass blowing flux. However, as the mass blowing flux in air is more substantial than in nitrogen, the blockage effect comes into play. The surface temperature is not significantly altered by the Schmidt number due to the competition between blockage (which reduces the convective heat flux) and oxidation (which increases the energy release at the surface), as both are increased with increasing mass flux. In conclusion, the Schmidt number cannot be responsible for the surface temperature overestimation for P-A-15-T1500 and underestimation for P-A-15-T2800.

(a) Mass blowing flux for the three test conditions

(b) Surface temperature for the three test conditions
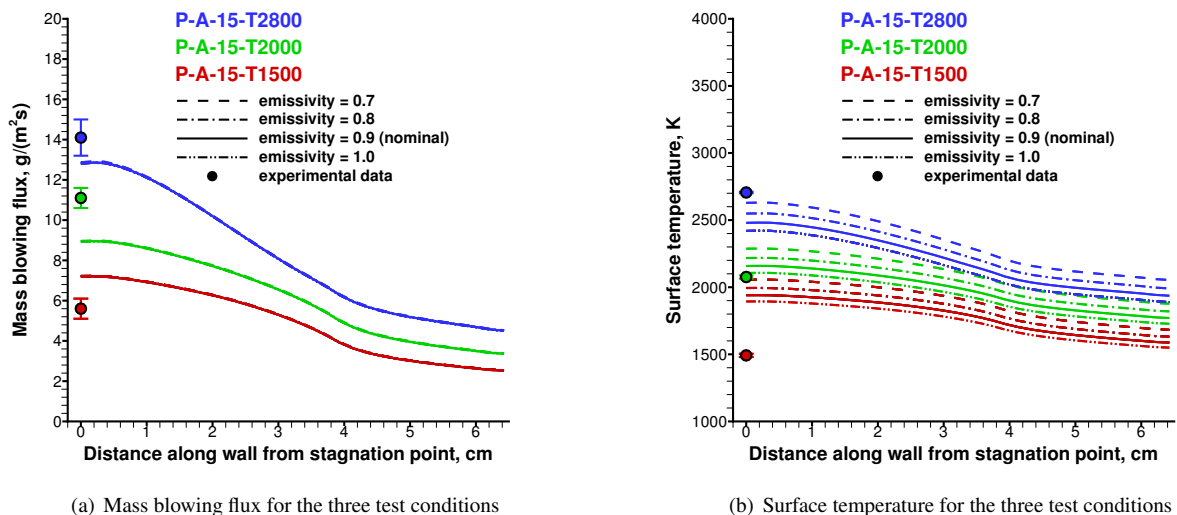
Figure 24: Distributions of mass blowing flux and temperature along the surface for varying surface emissivity.

The distributions of mass blowing flux and temperature along the sample surface for varying surface emissivity are shown in Fig. 24. The surface emissivity is practically not affecting the mass blowing flux. Differently, the effect of the the surface emissivity on the surface temperature is significant for all of the three cases, as shown in Fig. 24(b), as the emissivity is directly affecting the surface energy balance. The higher the surface emissivity, the lower the surface temperature. However, even considering surface emissivities as high as 1.0, the surface temperatures for P-A-15-T1500

NUMERICAL ANALYSIS OF CATALYSIS AND ABLATION EFFECTS FOR CARBON-BASED ABLATIVE MATERIALS

still result to be overestimated.

(a) Mass blowing flux for the three test conditions

(b) Surface temperature for the three test conditions
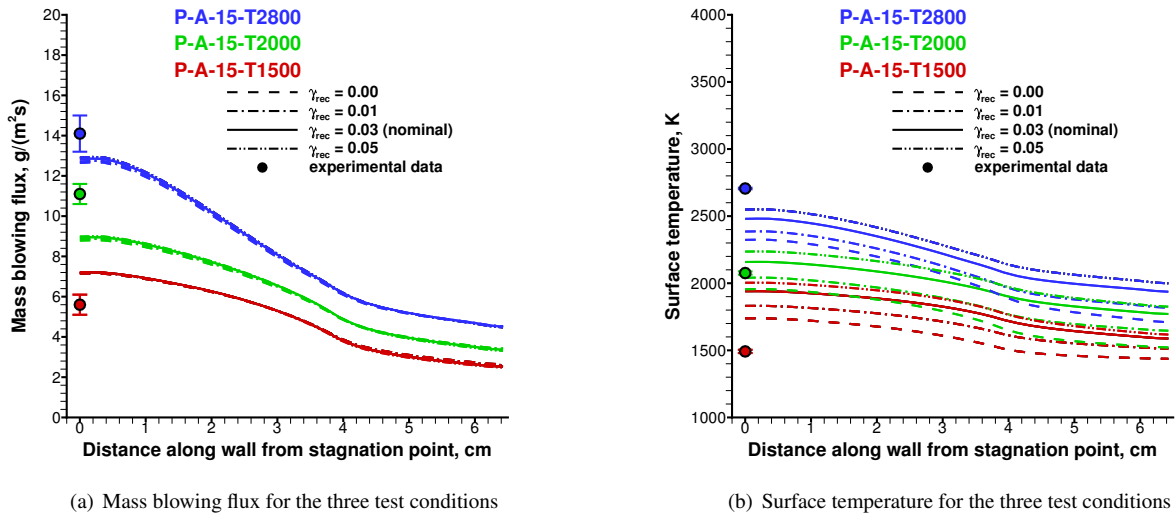
Figure 25: Distributions of mass blowing flux and temperature along the surface for varying recombination efficiency.

The distributions of mass blowing flux and temperature along the sample surface for varying recombination efficiency (γ_{rec}) are shown in Fig. 25. Nitrogen recombination efficiency is affecting dominantly the surface temperature, Fig. 25(b), and only marginally the mass blowing flux, Fig. 25(a). This is different from nitrogen cases, where mass blowing flux was also affected, as for air cases recession is dominated by carbon-oxygen reaction. The surface temperature is directly influenced by the recombination efficiency because of the associated significant heat of recombination: the higher the recombination efficiency, the higher the surface temperature. Computed results show that for null recombination efficiency the overestimation of surface temperatures for P-A-15-T1500 drops significantly passing from +30% down to +16%, although still resulting in an overprediction of the measured data.

(a) Mass blowing flux for the three test conditions

(b) Surface temperature for the three test conditions
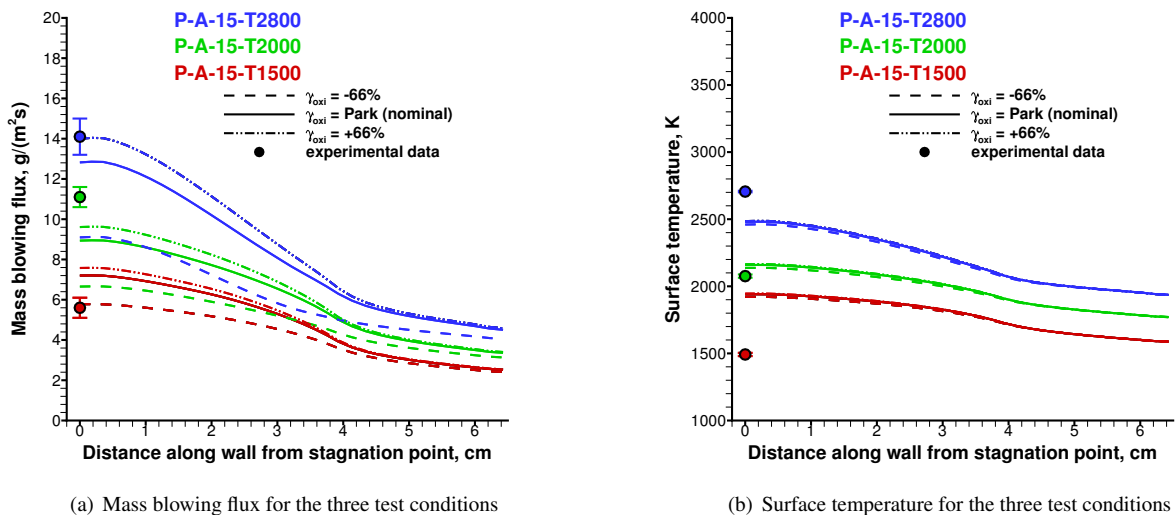
Figure 26: Distributions of mass blowing flux and temperature along the surface for varying oxidation efficiency.

The distributions of mass blowing flux and temperature along the sample surface for varying oxidation efficiency (γ_{oxi}) are shown in Fig. 26. Carbon oxidation efficiency is significantly affecting the mass blowing flux, Fig. 26(a), while it is practically not affecting the surface temperature, Fig. 26(b). The mass blowing flux is obviously directly influenced by the oxidation efficiency: the higher the oxidation efficiency, the higher the mass blowing flux. However, since carbon oxidation has been shown to be limited mostly by atomic oxygen diffusion rather than by its chemical

kinetics, an increase of γ_{oxi} only produces a small increase of $\dot{m}$ while an equal decrease of γ_{oxi} produces a much larger decrease of $\dot{m}$ because the oxidation reaction switches from diffusion- to kinetic-limited regime. The surface temperature is practically not influenced by the oxidation reaction because of the competition between blockage effect and oxidation heat of reaction (both are affected by $\dot{m}$), as already discussed in the analysis of the Schmidt number effect.

(a) Mass blowing flux for the three test conditions

(b) Surface temperature for the three test conditions
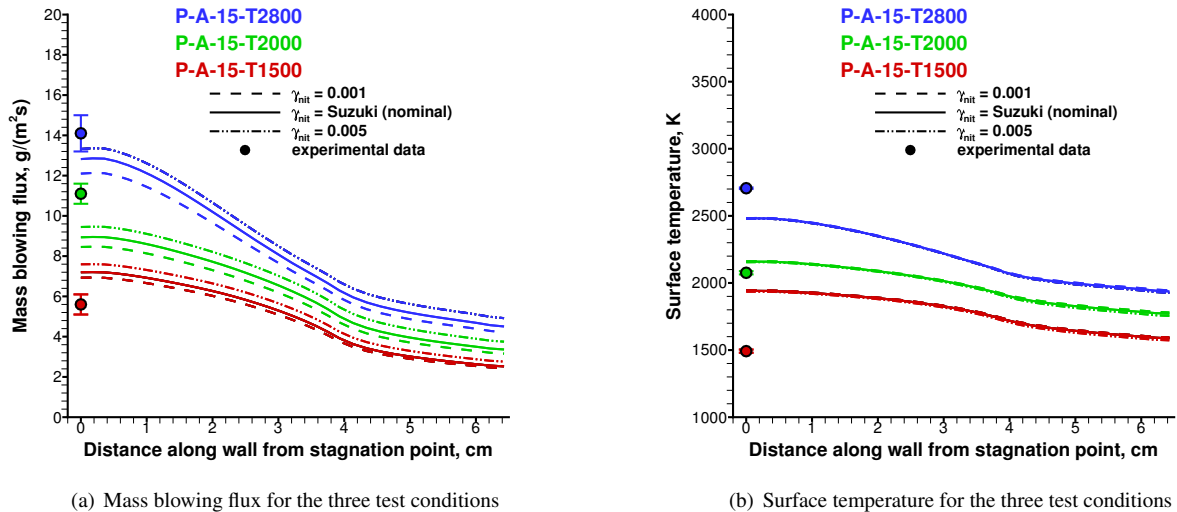
Figure 27: Distributions of mass blowing flux and temperature along the surface for varying nitridation efficiency.

Finally, the distributions of mass blowing flux and temperature along the sample surface for varying nitridation efficiency (γ_{nit}) are shown in Fig. 27. Carbon nitridation efficiency is only mildly affecting the mass blowing flux, Fig. 27(a), while it is practically not affecting the surface temperature, Fig. 27(b). The mass blowing flux is obviously directly influenced by the nitridation efficiency: the higher the nitridation efficiency, the higher the mass blowing flux. However, since mass blowing flux contribution from nitridation is minimal (90% of recession is due to oxidation), the effect of γ_{nit} on overall mass blowing flux is limited. In conclusion, due to the dominance of carbon oxidation, the effect of γ_{nit} on mass blowing flux is less important with respect to the much stronger effect of γ_{oxi}, as shown in Fig. 26(a). Lastly, the surface temperature is not influenced by the nitridation reaction because of the small heat of reaction associated with the carbon nitridation, as already noted for the nitrogen cases. Note that the possibility of atomic oxygen recombination has not been taken into consideration. The reasons for this choice are, first, that there is no experimental evidence in the open literature of atomic oxygen recombining at a carbon surface and, second, that mostly of the available oxygen is consumed by the oxidation reaction.

The thorough sensitivity analysis that has been performed for air tests revealed that the surface temperature is primarily affected by the recombination efficiency and secondarily by the surface emissivity (exactly the same as for nitrogen tests). On the other hand, the surface recession is primarily affected by both the oxidation efficiency and the Schmidt number (as oxidation appears to be close to the diffusion-limited regime in the analyzed conditions) and secondarily by the nitridation efficiency, as it can only affect that $\approx 10\%$ of mass blowing flux. Moreover, the sensitivity analysis also confirmed that both nitridation and oxidation efficiencies have no significant impact on wall temperature.

3.4 Extraction of effective reaction probabilities

For nitrogen cases the sensitivity analysis showed that the experimental data on the surface temperature can be practically exploited to get insight into the recombination efficiency while the experimental data on the mass blowing flux can be exploited to get insight into the nitridation efficiency. However, as the recombination efficiency has been also shown to indirectly affect the mass blowing flux (because of the competition between nitridation and recombination reactions), the two efficiencies, γ_{rec} and γ_{nit}, must be solved for in a coupled manner. For air cases, on the other hand, the experimental data on the surface temperature can be practically exploited to get insight into the recombination efficiency while the experimental data on the mass blowing flux can be exploited to get insight into the oxidation efficiency, using the nitridation efficiency, γ_{nit}, derived from pure nitrogen tests. The two efficiencies, γ_{rec} and γ_{oxi}, must be solved for in a coupled manner.

NUMERICAL ANALYSIS OF CATALYSIS AND ABLATION EFFECTS FOR CARBON-BASED ABLATIVE MATERIALS

Hence, according to the conclusion drawn from the sensitivity analysis, an "inverse approach" can be defined to derive, directly from the CFD solution, the effective reaction probabilities for the reactions under scrutiny for pure nitrogen test cases and for air test cases based on the experimentally measured data. For nitrogen cases, by assuming $\dot{m}_w = \dot{m}_{w,\exp}$ and $T_w = T_{w,\exp}$ the energy equation can be solved for γ_{rec}, coupled with the species mass balance equations, Eq. 1, to solve for the surface chemical composition, y_{i_w}. Once the surface mass and energy equations are jointly solved (in an iterative fashion), γ_{nit} can be directly calculated from Eq. 2, using the atomic nitrogen mass fraction, y_N, computed from the surface chemical composition. For air cases, by assuming $\dot{m}_w = \dot{m}_{w,\exp}$ and $T_w = T_{w,\exp}$ and using the previously calculated γ_{nit} value, the energy equation can be solved for γ_{rec}, coupled with the species mass balance equations, Eq. 1, to solve for the surface chemical composition, y_{i_w}. Once the surface mass and energy equations are jointly solved (in an iterative fashion), γ_{oxi} can be directly calculated from Eq. 2, using the previously calculated γ_{nit} and the atomic nitrogen and atomic oxygen mass fraction, y_N and y_O, computed from the surface chemical composition. As the experimental measurement are only available at the stagnation point, the "cut-out" grid is used for the following analysis.

The results from the "inverse approach" in terms of effective reaction probabilities for carbon nitridation and nitrogen recombination at the stagnation point of the carbon preform for the pure nitrogen cases are discussed first. A sensitivity analysis to the most important parameters that have been identified is also included. In the "inverse approach", the reaction probabilities are the outcome of the procedure so that the sensitivity analysis reduces to: Schmidt number and surface emissivity. Three Schmidt numbers have been considered, namely 0.5, 0.7 (reference) and 0.9 and four surface emissivities have been considered, namely 0.7, 0.8, 0.9 (reference) and 1.0.
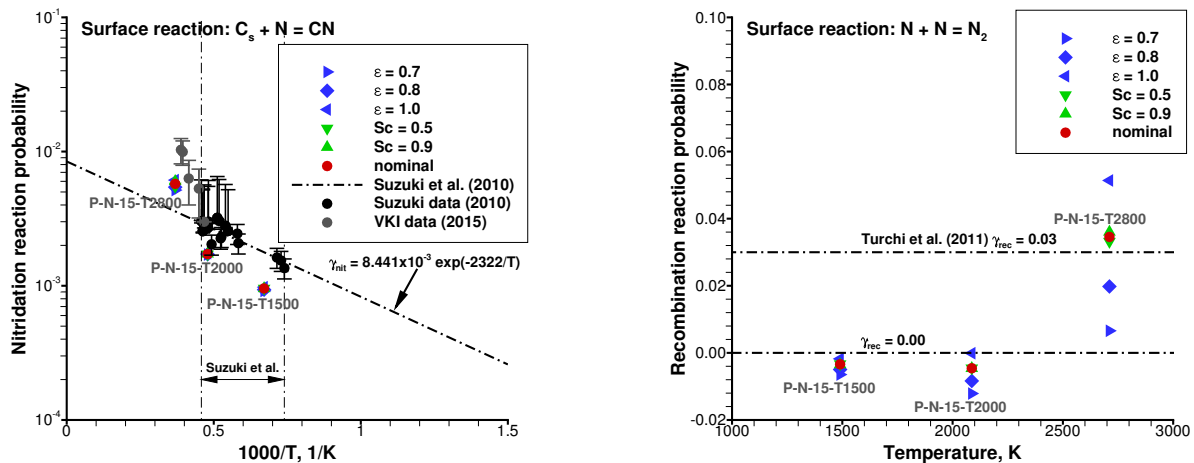
(a) Carbon nitridation reaction probability (log-scale) as a function of inverse temperature including data from Ref. (16) and from Ref. (19)

(b) Nitrogen recombination reaction probability as a function of temperature including data from Ref. (19)

Figure 28: Nitridation and recombination reaction probabilities vs temperature for varying Schmidt number and surface emissivity for pure nitrogen tests.

Figure 28 shows the numerically derived nitridation and recombination reaction probabilities vs temperature for varying Schmidt number and surface emissivity. The nitridation reaction probability, Fig. 28(a), appears to be in the range 0.001 - 0.005, in agreement with the recent literature.[16, 19] The nitridation probability is also shown to increase with temperature in good agreement with the regression expression in the Arrhenius form proposed by Suzuki et al.[?] Is is also interesting to note that the derived nitridation probability is negligibly affected by the Schmidt number, as the nitridation reaction has been shown to be in the kinetic limited regime. The effect of the surface emissivity on the nitridation probability is also shown to be extremely limited, with some small effect only visible at the highest surface temperature, for P-N-15-T2800. The derived probabilities are therefore modestly affected by the analyzed parameters so the scattering of results is mostly limited. The nitrogen recombination reaction probability, shown in Fig. 28(b), appears to be in the range 0.00 - 0.04, in agreement with recent experimental work.[10, 19] The recombination probability appears to be negligibly small for low to mid surface temperatures, P-N-15-T1500 and P-N-15-T2000 test cases, and rise significantly for the highest surface temperature case, P-N-15-T2800. Note that for some conditions (mainly depending on the assumed surface emissivity), the calculated probability becomes negative, indicating a dissociation of molecular nitrogen at the surface. Is it also interesting to note that the species diffusion, through the Schmidt number, has practically no or very limited effect on the derived recombination probability. On the other hand, surface
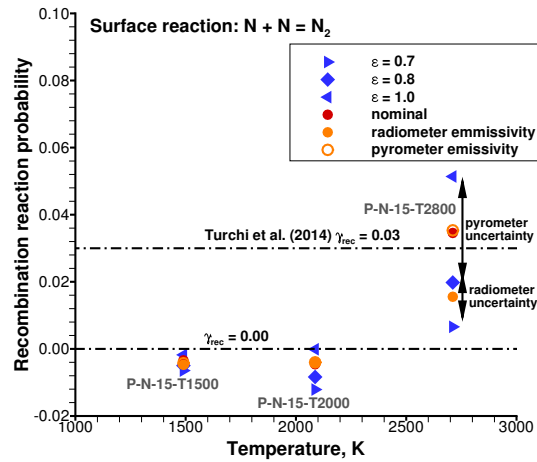
Figure 29: Nitrogen recombination reaction probability vs temperature for varying surface emissivity including radiometer and pyrometer data.

emissivity is significantly affecting the results, especially at the higher surface temperatures where the re-radiation flux becomes dominant, hence strongly enhancing the effect of material emissivity on the solution. At the highest surface temperature, for test case P-N-15-T2800, by varying the surface emissivity from 0.7 to 1.0 (equivalent to a black body) the reconstructed recombination probability passes from a minimum value of 0.006 to a maximum value of 0.05, hence increasing by almost one order of magnitude.

It is worth noting that the carbon preform surface emissivity for each experimental test case has been measured during the test using both a pyrometer and a radiometer. Results for nitrogen recombination reaction probability vs temperature for varying surface emissivity and including the data from the radiometer and pyrometer (including their measurement errors) are reported in Fig. 29 (as the Schmidt number effect has been shown to affect the solution in a negligible way, it has not been reported here). The derived nitridation probability is not shown as it is practically the same when using radiometer or pyrometer emissivities. Only at the highest surface temperature, for test case P-N-15-T2800, a very limited scatter is visible with an probability of 0.0053 when using the radiometer data and of 0.0058 when using the pyrometer data. This, again, confirms that the scattering of results for nitridation probability is mostly limited. Differently, the scattering of results appear significant, at the highest surface temperature, when looking at the derived recombination probability, shown in Fig. 29. For the low and mid surface temperature cases, P-N-15-T1500 and P-N-15-T2000, in fact, the recombination probability appears to be practically zero with no scattering. However, for P-N-15-T2800, the recombination probability is strongly scattered and results obtained using radiometer or pyrometer are visibly different. The derived probability is 0.016 when using the radiometer data and rises up to 0.035 (more than twice) when using the pyrometer data. Nevertheless, both values can be considered in line with literature data,[10,19] that are scattered as well. Is is also important to note that the effect of the measurement error of the instrument is significant on the solution, especially when the pyrometer is used, due to its higher error.

The results from the "inverse approach" in terms of effective reaction probabilities for carbon oxidation and nitrogen recombination at the stagnation point of the carbon preform for the air cases are now discussed. A sensitivity analysis to the most important parameters that have been identified is also included. As for the pure nitrogen analysis, three Schmidt numbers have been considered, namely 0.5, 0.7 (reference) and 0.9 and four surface emissivity have been considered, namely 0.7, 0.8, 0.9 (reference) and 1.0.

Figure 30 shows the numerically derived oxidation and recombination reaction probabilities vs temperature for varying Schmidt number and surface emissivity. The carbon oxidation reaction probability, shown in Fig. 30(a), appears to be in the range 0.1 - 0.7, with a clear dependence on surface temperature, hence two orders of magnitude higher than the previously derived nitridation probability, again confirming that in air environment carbon recession is dominated by the oxidation reaction. The oxidation probability is shown to increase with temperature in fair agreement with the regression expression in the Arrhenius form proposed by Park et al.[13] Is is also important to note that, differently from the previously derived nitridation probability, the calculated oxidation probability is significantly affected by the Schmidt number, as the oxidation reaction has been shown to be in or very close to the diffusion limited regime. The effect of the surface emissivity on the oxidation probability is, on the other hand, shown to be extremely limited, with some small effect only visible at the highest surface temperature, for P-A-15-T2800, analogously to what shown

NUMERICAL ANALYSIS OF CATALYSIS AND ABLATION EFFECTS FOR CARBON-BASED ABLATIVE MATERIALS
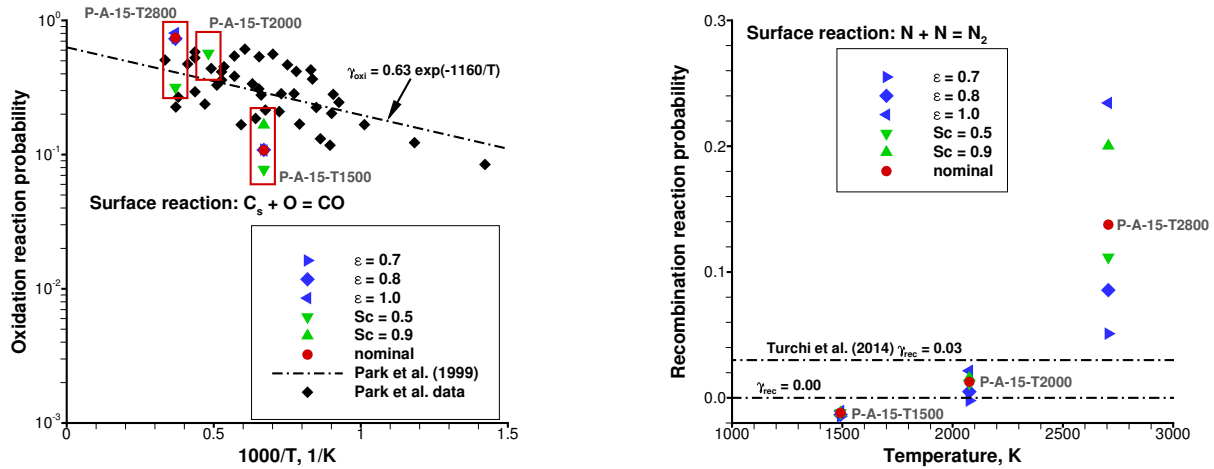
(a) Carbon oxidation reaction probability (log-scale) as a function of inverse temperature including data from Ref. (13)

(b) Nitrogen recombination reaction probability as a function of temperature including data from Ref. (19)

Figure 30: Oxidation and recombination reaction probabilities vs temperature for varying Schmidt number and surface emissivity for air tests.
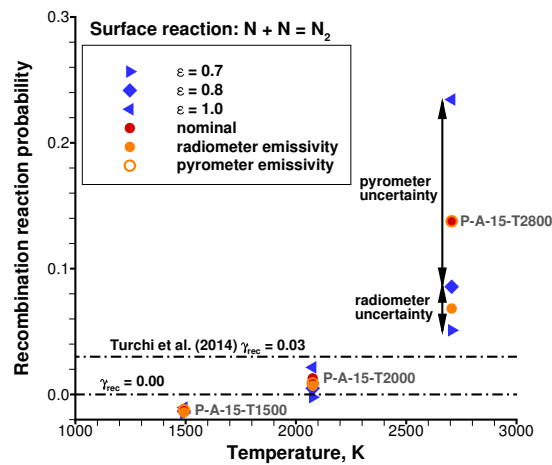
Figure 31: Nitrogen recombination reaction probability vs temperature for varying surface emissivity including radiometer and pyrometer data.

for nitridation in pure nitrogen cases. The derived oxidation probabilities are therefore strongly affected by the sole Schmidt number and the scattering of results is quite evident. In particular, for some conditions, the procedure does not converge to physical solutions as oxidation probabilities required to match the experimental mass blowing rate are higher than one. The meaning of these solutions is that, being the oxidation in a diffusion-limited regime, it is not possible to further increase recession rate to match the experimental data by acting on the reaction probability. Such non-physical solutions are obtained for P-A-15-T2000 for Schmidt numbers of 0.7 (for all emissivities) and 0.9 and for P-A-15-T2800 for Schmidt number of 0.9. The consequence of this fact is that it appears much more difficult to derive information in terms of reaction efficiency when the reaction under scrutiny lies in a diffusion-limited regime, as it becomes basically almost insensitive to a reaction rate variation. That is the reason why the derived oxidation probabilities are much more scattered if compared to the previously derived nitridation probabilities, that appeared closely grouped.

The nitrogen recombination reaction probability, shown in Fig. 30(b), appears to be in the range 0.00 - 0.01 for P-A-15-T1500 and P-A-15-T2000, in agreement with recent experimental work.[19] However, for for P-A-15-T2800,

the nitrogen recombination reaction probability appears extremely scattered with an even higher scattering than for P-N-15-T2800. Differently from the nitrogen cases, where the Schmidt number was not affecting the recombination probabilities, for air cases both the surface emissivity and the Schmidt number are affecting the results, in that order. The recombination probability appears to be small for low to mid surface temperatures, P-A-15-T1500 and P-A-15-T2000 test cases, and rises significantly for the highest surface temperature case, P-A-15-T2800. Note that for some conditions (mainly depending on the assumed surface emissivity), especially at the lowest surface temperature, the calculated probability becomes negative, indicating a dissociation of molecular nitrogen at the surface (this results has been experienced also for some nitrogen test cases). At the highest surface temperature, for test case P-A-15-T2800, by varying the surface emissivity from 0.7 to 1.0 (equivalent to a black body) the reconstructed recombination probability passes from a minimum value of 0.05 to a maximum value of 0.23, hence increasing by almost five times.

Results for recombination reaction probabilities vs temperature for varying surface emissivity and including the data from the radiometer and pyrometer (including their measurement errors) are reported in Fig. 31. As shown, at the highest surface temperature, the scattering of results appear significant. For the low and mid surface temperature cases, P-A-15-T1500 and P-A-15-T2000, in fact, the recombination probability appears to be close to zero with limited scattering (especially for the lowest temperature case, P-A-15-T1500). However, for P-A-15-T2800, the recombination probability is extremely scattered and results obtained using radiometer or pyrometer are significantly different. The derived probability is 0.06 when using the radiometer data and rises up to 0.14 (more than twice) when using the pyrometer data. As for the pure nitrogen tests, the effect of the measurement error of the instrument is extremely significant on the solution, especially when the pyrometer is used, due to its higher error.
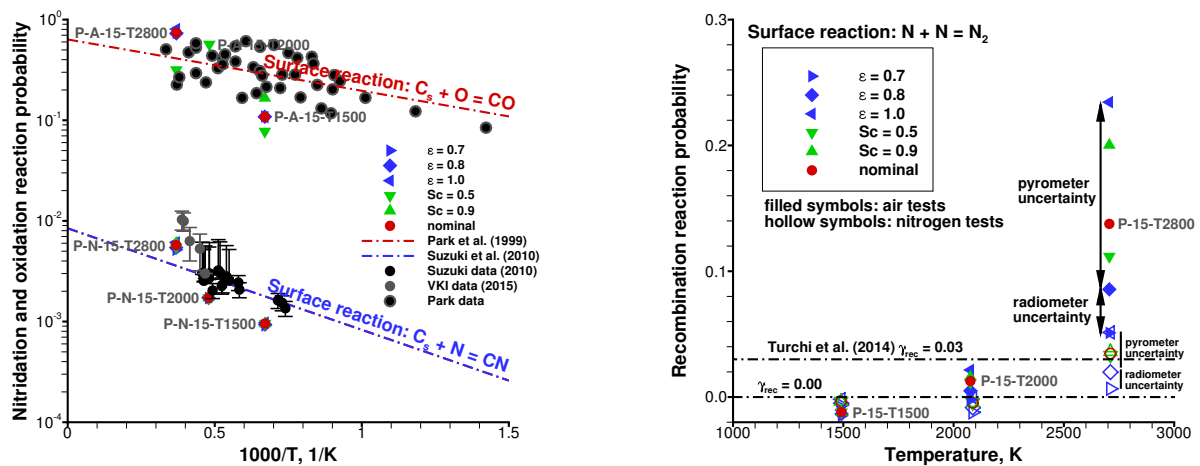
(a) Carbon oxidation and nitridation reaction probability (log-scale) as a function of inverse temperature for both pure nitrogen and air cases

(b) Nitrogen recombination reaction probability as a function of temperature for both pure nitrogen and air cases

Figure 32: Oxidation, nitridation, and recombination reaction probabilities vs temperature for varying Schmidt number and surface emissivity for both pure nitrogen and air cases.

Finally, Fig. 32 shows the oxidation, nitridation, and recombination reaction probabilities vs temperature for varying Schmidt number and surface emissivity for both pure nitrogen and air cases. As shown in Fig. 32(a), carbon oxidation probability is two orders of magnitude larger than carbon nitridation probability. Both probabilities are fairly in line with available experimental data, although oxidation data present a significant scatter, due to the diffusion limited regime of the surface reaction, for the analyzed operating conditions. Concerning the nitrogen recombination probability, both pure nitrogen and air cases at low to mid surface temperatures, are consistent in showing null to limited reaction probabilities. However, at the highest surface temperature, for both pure nitrogen and air cases, the recombination probability becomes visible although showing a significant scattering due to the uncertainty in the surface emissivity, which is even more evident for the air case.

4. Conclusions

The numerical simulations that have been performed for carbon preform in pure nitrogen and air environments to derive the carbon nitridation/oxidation and nitrogen recombination probabilities from the proposed procedure have shown

that: i) carbon nitridation probability can be reconstructed with a very limited scatter; ii) carbon oxidation probability can be reconstructed with a significant scatter due to the diffusion modeling uncertainty (i.e. Schmidt number); and iii) nitrogen recombination probability is strongly affected by the emissivity measurement errors at the highest wall temperature. The nitridation probability appears to be negligibly affected by both the diffusion model (through the Schmidt number) and the surface emissivity. Obtained results from the joint numerical/experimental rebuild appears to be in the range 0.001 - 0.005 and are quite in line with recent literature data. The oxidation probability, on the other hand, appears to be negligibly affected by the surface emissivity but significantly affected by the diffusion model, through the Schmidt number. Obtained results from the joint numerical/experimental rebuild appears to be in the range 0.1 - 0.7 and, despite the scatter, are fairly in line with literature data. It is worth stressing that, for an accurate reconstruction of the carbon oxidation probability, a kinetic limited oxidation regime is desired. However, due to the significantly higher reaction probability of oxidation with respect to nitridation reaction and due to the reduced oxygen content in the environmental gas (air), simulations confirmed that oxidation reaction lies in or very close to the diffusion limited regime. When such a condition applies, it becomes extremely difficult to derive useful information in terms of reaction rate constants and probabilities, as the mass blowing flux becomes more and more insensitive to these parameters. Therefore, it is suggested to perform tests in operational conditions such that carbon oxidation lies in a kinetic limited regime, as experienced for carbon nitridation in pure nitrogen environment. One option to obtain such a condition is to reduce surface temperature, which, however, would not allow to test the oxidation reaction at the high surface temperatures that can be interesting for the reentry community. Another option would be that of making experiments in a pure oxygen environment, that would significantly increase the oxygen content in the environmental gas with respect to an air environment, possibly shifting the oxidation regime from diffusion-limited to kinetic-limited. From pure nitrogen tests, nitrogen recombination probability is shown to be negligibly small (or even negative) for low to mid surface temperature cases (1500 and 2000 K) while it assumes positive values in the range 0.016 - 0.035 at the highest surface temperature (2800 K), depending on which instrument is used to derive the surface emissivity (radiometer or pyrometer). The above mentioned values are in agreement with recombination probabilities over carbon surface present in the open literature, which lies in the range 0.03 - 0.035. For air cases, nitrogen recombination probability is shown to be negligibly small (or even negative) for low to mid surface temperature cases, somewhat similar to what derived for pure nitrogen tests. At the highest surface temperature, however, it has been shown that the uncertainty in the measured surface emissivity result in a very large scatter of the reaction probability, ranging from 0.06 when using the radiometer data and up to 0.14 (more than twice) when using the pyrometer data. Again, as concluded for the nitrogen tests, it is important to stress here the importance of trying to reduce as much as possible the measurement error on the surface emissivity, in order to be able to derive with improved accuracy the nitrogen recombination probability at higher surface temperatures, where the re-radiation flux becomes a dominant term in the surface energy balance.

Acknowledgments

References

[1] D. Bianchi and F. Nasuti. Numerical analysis of nozzle material thermochemical erosion in hybrid rocket engines. *Journal of Propulsion and Power*, 29(3):547–558, 2013. doi: 10.2514/1.B34813.

[2] D. Bianchi, F. Nasuti, and E. Martelli. Navier-stokes simulations of hypersonic flows with coupled graphite ablation. *Journal of Spacecraft and Rockets*, 47(4):554–562, 2010. doi: 10.2514/1.47995.

[3] D. Bianchi, F. Nasuti, and M. Onofri. Aerothermodynamic analysis of reentry flows with coupled ablation. AIAA Paper 2011-2273, 2011. doi: 10.2514/6.2011-2273.

[4] D. Bianchi, F. Nasuti, M. Onofri, and E. Martelli. Thermochemical erosion analysis for graphite/carbon-carbon rocket nozzles. *Journal of Propulsion and Power*, 27(1):197–205, 2011. doi: 10.2514/1.47754.

[5] D. Bianchi, F. Nasuti, R. Paciorri, and M. Onofri. Computational analysis of hypersonic flows including finite rate ablation thermochemistry. In Proc. 7th European Workshop on Thermal Protection Systems and Hot Structures, April 2013, ESA SP-. Noordwijk, The Netherlands, ESA-ESTEC.

[6] D. Bianchi, F. Nasuti, R. Paciorri, and M. Onofri. Hypersonic flow analysis including finite rate ablation thermochemistry. In Proc. 5th European Conference for Aeronautics and Space Sciences. Munich, Germany, 2013.

[7] D. Bianchi, A. Turchi, F. Nasuti, and M. Onofri. Chemical erosion of carbon-phenolic rocket nozzles with finite-rate surface chemistry. *Journal of Propulsion and Power*, 29(5):1220–1230, 2013. doi: 10.2514/1.B34791.

[8] G. Duffa. Ablative thermal protection systems modeling. *AIAA Education Series*, 2013. Reston, Virginia.

[9] P. A. Gnoffo, K. J. Weilmuenster, H. H. Hamilton, D. R. Olynick, and E. Venkatapathy. Computational aerothermodynamic design issues for hypersonic vehicles. *Journal of Spacecraft and Rockets*, 36(1), 1999.

[10] B. Helber, A. Turchi, and T. E. Magin. Determination of active nitridation reaction efficiency of graphite in inductively coupled plasma flows. *Carbon*, 125(1), 2017.

[11] R. M. Kendall, R. A. Rindal, and E. P. Bartlett. Thermochemical ablation. *AIAA Paper*, 642(100), 1965.

[12] B. Laub and E. Venkatapathy. Thermal protection system technology and facility needs for demanding future planetary missions. In Proc. International Workshop on Planetary Probe Atmospheric Entry and Descent Trajectory Analysis and Science, 2004, ESA SP-544. Noordwijk, The Netherlands, ESA-ESTEC.

[13] C. Park and H. K. Ahn. Stagnation-point heat transfer rates for pioneer-venus probes. *Journal of Thermophysics and Heat Transfer*, 13(1), 1999.

[14] H. Ritter. Development of a european ablative material for heatshields of sample return missions. In Proc. 6th European Workshop on Thermal Protection Systems and Hot Structures. Stuttgart, Germany, 2009.

[15] G. W. Sutton. The initial development of ablation heat protection, an historical perspective. *Journal of Spacecraft and Rockets*, 19(1), 1982.

[16] T. Suzuki, K. Fujita, and T. Sakai. Experimental study of graphite ablation in nitrogen flow, part ii: Further numerical analysis. *Journal of Thermophysics and Heat Transfer*, 24(3):589–597, 2010. doi: 10.2514/1.43264.

[17] H. K. Tran. Development of light weight ceramic ablators and arc-jet test results. National Aeronautics and Space Administration, Ames Research Center, 1994.

[18] A. Turchi, D. Bianchi, F. Nasuti, and M. Onofri. A numerical approach for the study of the gas-surface interaction in carbon-phenolic solid rocket nozzles. *Aerospace Science and Technology*, 27(1):25–31, 2013. 10.1016/j.ast.2012.06.003.

[19] A. Turchi, B. Helber, A. Munafò, and T. E. Magin. Development and testing of an ablation model based on plasma wind tunnel experiments. AIAA Paper 2014-2125, 2014.